Mesospheric Non-Migrating Tides Generated With Planetary Waves: I Characteristics

H. G. Mayr, J. G. Mengel., E. L. Talaat, H. S. Porter, K. L. Chan
[1]Goddard Space Flight Center, Greenbelt, MD, 20771
[2]Science Systems & Applications, Inc., Lanham, MD
[3]Applied Physic Laboratory, Johns Hopkins University, Laurel, MD
[4]Furman University, Greenville, SC
[5]Hong Kong University of Science and Technology, Hong Kong, China

Prepared

for

Journal of Atmospheric and Solar Terrestrial Physics

July, 2003

Mesospheric Non-Migrating Tides Generated With Planetary Waves: I Characteristics

H. G. Mayr, J. G. Mengel., E. L. Talaat, H. S. Porter, K. L. Chan
[1]Goddard Space Flight Center, Greenbelt, MD, 20771
[2]Science Systems & Applications, Inc., Lanham, MD
[3]Applied Physic Laboratory, Johns Hopkins University, Laurel, MD
[4]Furman University, Greenville, SC
[5]Hong Kong University of Science and Technology, Hong Kong, China

Popular Summary: For comparison with measurements from the TIMED mission and supporting ground-based observations, we discuss results from a modeling study with our Numerical Spectral Model (NSM) that specifically deals with the non-migrating tides generated in the mesosphere. The NSM extends from the ground to the thermosphere, incorporates Hines' Doppler Spread Parameterization for small-scale gravity waves (GWs), and it describes the major dynamical features of the atmosphere including the wave driven equatorial oscillations (QBO and SAO), and the seasonal variations of tides and planetary waves. Accounting solely for the excitation sources of the solar migrating tides, the NSM generates through dynamical interactions also non-migrating tides in the mesosphere that are comparable in magnitude to those observed. Large non-migrating tides are produced in the diurnal and semi-diurnal oscillations for the zonal mean (m = 0) and in the semidiurnal oscillation for m = 1. In general, significant eastward and westward propagating tides are generated for all the zonal wave numbers m = 1 to 4. To identify the cause, the NSM is run without the solar heating for the zonal mean (m = 0), and the amplitudes of the resulting non-migrating tides are then negligibly small. In this case, the planetary waves are artificially suppressed, which are generated in the NSM through instabilities. This leads to the conclusion that the non-migrating tides are generated through non-linear interactions between planetary waves and migrating tides, as had proposed. In an accompanying paper (Part II), we present results from numerical experiments, which indicate that gravity wave filtering contributes significantly to produce the non-linear coupling that is involved.

Abstract: We discuss results from a modeling study with our Numerical Spectral Model (NSM) that specifically deals with the non-migrating tides generated in the mesosphere. The NSM extends from the ground to the thermosphere, incorporates Hines' Doppler Spread Parameterization for small-scale gravity waves (GWs), and it describes the major dynamical features of the atmosphere including the wave driven equatorial oscillations (QBO and SAO), and the seasonal variations of tides and planetary waves. Accounting solely for the excitation sources of the solar migrating tides, the NSM generates through dynamical interactions also non-migrating tides in the mesosphere that are comparable in magnitude to those observed. Large non-migrating tides are produced in the diurnal and semi-diurnal oscillations for the zonal mean (m = 0) and in the semidiurnal oscillation for m = 1. In general, significant eastward and westward propagating tides are generated for all the zonal wave numbers m = 1 to 4. To identify the cause, the NSM is run without the solar heating for the zonal mean (m = 0), and the amplitudes of the resulting non-migrating tides are then negligibly small. In this case, the planetary waves are artificially suppressed, which are generated in the NSM through instabilities. This leads to the conclusion that the non-migrating tides are generated through non-linear interactions between planetary waves and migrating tides, as Forbes et al. and Talaat and Liberman had proposed. In an accompanying paper, we present results from numerical experiments, which indicate that gravity wave filtering contributes significantly to produce the non-linear coupling that is involved.

I. Introduction

Measurements from the ground (e.g., Avery et al., 1989; Manson et al., 1989; Vincent et al., 1989) and with the UARS spacecraft (Hays et al., 1994; McLandress et al., 1996; Burrage et al., 1995a, b) have shown that the diurnal tides in the mesosphere and lower thermosphere exhibit large seasonal variations, which are modulated by planetary waves (e.g., Forbes, 1995, Fritts, 1995a, b). The amplitude of the fundamental diurnal tide exhibits large maxima during equinox, which have been attributed to postulated variations in eddy viscosity (e.g., Geller et al., 1997; Yudin et al., 1997), and to variations in eddy viscosity associated with gravity wave interaction (Akmaev, 2001a).

In the Numerical Spectral Model (NSM) discussed here, the seasonal variations of the fundamental diurnal tide were attributed also to gravity wave (GW) momentum deposition and

filtering by the mean zonal circulation (Mayr et al., 1998, 2001a). The seasonal variations of the semi-diurnal tide were shown to be affected by non-linear interactions with the diurnal tide, which was attributed to gravity wave filtering (Mayr et al., 1999, 2001a). Planetary waves generated internally by the baroclinic instability and GW forcing (Mayr et al., 2001b) were shown to produce large amplitude modulations of the diurnal and semi-diurnal tides.

The above observations and modeling results refer mainly to the dominant westward migrating tides. In the upper mesosphere, however, the nonmigrating tides are also important. Forbes et al. (1995) observed a westward propagating 12-hour wave in the radar measurements near the north pole and suggested that it is produced by nonlinear interactions between the solar driven migrating semidiurnal tide and stationary m = 1 planetary waves. Based on an analysis of UARS High Resolution Doppler Imager (HRDI) measurements over a period of four years, Talaat and Lieberman (1999) observed in the diurnal (24 hour) tide above 80 km large amplitudes at zonal wave number m = 0 and nonmigrating components at m = 1 – 3 that were as large as the migrating tide during some seasons.

The inferred phase structure of the nonmigrating tides generally suggests that they propagate up from below (Lieberman, 1991; Talaat and Lieberman, 1999). However, the forcing of these tides – due to solar insolation of tropospheric water vapor and stratospheric ozone (the main sources for migrating tides), and latent heat release as well as convective or sensible heating – cannot produce the observed amplitudes (e.g., Miyahara et al., 1993; Hagan et al., 1997). As an alternative means for generating nonmigrating tides, Waltersheid et al. (1986) suggested that gravity wave interactions with migrating tides could be important, and Teitelbaum and Vial (1991) proposed non-linear interactions between migrating tides and planetary waves. Miyahara et al. (1999) found that nonlinear interactions between waves could produce the nonmigrating tides in their model. Simulations with the TIME-GCM model, Hagan and Roble (2001) suggested that non-linear interactions between the migrating diurnal tide and m = 1 planetary waves could produce non-migrating tides in the upper mesosphere.

We recently demonstrated that this mechanism generates the m = 0 diurnal tide in our model (Mayr et al., 2003), and the amplitudes were shown to be comparable to those observed in the mesosphere. The purpose of the present paper is to describe more fully the non-migrating tides. We shall elaborate on the planetary wave mechanism and discuss the characteristics and seasonal variations of these tides. In an accompanying paper (Part II), we shall present the

results of numerical experiments that reveal the role gravity waves play in generating the nonlinear interactions that produce the non-migrating tides.

II. Numerical Spectral Model

The design of the Numerical Spectral Model (NSM) was introduced by Chan et al. (1994), and 2D as well as 3D versions of the model were employed to study a number of aspects of the middle atmosphere dynamics (e.g., Mengel et al., 1994; Mayr et al., 1997, 1998, 2001).

The NSM is non-linear, time dependent, and it is formulated with vector spherical harmonics. The model thus delineates the dynamical components in terms of zonal wave numbers, m. This yields for the zonal mean (m = 0), the seasonal variations (Annual Oscillation, AO; Semi-annual Oscillation, SAO) and the Quasi-biennial Oscillation (QBO); and for $m \geq 1$, the tides and planetary waves.

In the NSM, the nonlinear Navier Stokes equations are solved to describe the variations around the global mean of temperature and density, covering the atmosphere from the ground up to 400 km (240 km in the present application to speed up computation). Marching in time, the state variables are derived for the spherical harmonics and then synthesized to produce the solutions. The non-linear terms and the non-linear GW parameterization are evaluated in physical space.

Apart from GWs, the NSM presented here is driven by: (1) solar heating for the zonal mean (m = 0) component due to UV radiation in the mesosphere and stratosphere taken from Strobel (1978), and due to EUV radiation to describe the thermosphere, (2) the heating rates in the middle atmosphere and troposphere, taken from Forbes and Garrett (1978) and Forbes et al. (1997) to generate the migrating solar tides (diurnal and semi-diurnal). The radiative loss in the model is described in terms of Newtonian cooling, which was originally taken from Wehrbein and Leovy (1982) and Fels (1982). More recently, we have applied in our model the cooling parameterization of Zhu (1989).

The 3-D version of the NSM discussed here differs from the earlier version in that tropospheric heating in the zonal mean (m = 0) is applied (Held and Hou, 1980; Lindzen and Hou, 1988; Plumb and Hou, 1992) to reproduce qualitatively the observed zonal jets near the tropopause and the accompanying latitudinal temperature variations. Following Dunkerton (1997), we earlier applied such a heat source in our 2-D version of the NSM (Mayr et al.,

2001b) to study its affect on the wave driven equatorial oscillations (QBO, SAO). In 3-D, this additional heat source also produces planetary waves, which propagate from the troposphere into the mesosphere. The planetary waves that appear in the NSM are solely excited by instabilities, i.e., no planetary wave source of any kind is prescribed.

An integral part of the NSM is that it incorporates the Doppler Spread Parameterization (DSP) for small-scale GWs, formulated by Hines (1997, a, b), which is based on a theory developed in a series of papers (Hines, 1991a, b, c; 1993; 1996). Hines (2001, 2002) and Hines et al. (2002) further solidified the theoretical foundation of the DSP, which deals with a spectrum of waves that interact with each other to produce Doppler spreading. This in turn affects the interaction of the waves with the background flow, which is important for the dynamics of the middle atmosphere. The DSP has also been applied successfully in a variety of other global-scale models (e.g., Akmaev, 2001b; Manzini et al., 1997) and has been discussed extensively in the literature.

The wave-wave and wave-mean-flow interactions in the DSP are parameterized with Φ_1 and Φ_2 respectively, which are presently chosen in the model from the middle of the range recommended by the DSP. The GW source spectrum at the initial height varies like m^s, with $2 > s > 1$. We have been choosing $s = 1$ and introduce a cut-off minimum wave number of about $m_m = (2\ \text{km})^{-1}$ in accordance with the DSP. This cut-off in the GW source spectrum causes the wave momentum source and related eddy diffusivity to level off at altitudes above 80 km.

Assuming that the GW source at the initial height is isotropic, the momentum flux there is proportional to $\sigma_{hi}{}^3 k*$, where $k*$ is the characteristic horizontal wave number in the range $(100\ \text{km})^{-1} < k* < (10\ \text{km})^{-1}$. A value of $k* = (125\ \text{km})^{-1}$ is chosen. For the GW induced horizontal wind variability, we have chosen $\sigma_{hi} = 3$ m/s at 20 km, independent of latitude. In reality, the wave activity does change with latitude, as shown from observations by Allen and Vincent (1995) who report that σ_h increases at 20 km from about 2 m/s at mid latitudes to 3 m/s at the equator.

The DSP assures conservation of GW momentum and energy, and this requires at each altitude, latitude and longitude that a system of nonlinear equations be solved involving GW parameters, background winds, and Brunt Vaisala frequency. The equations are solved with Newtonian iteration, and convergence is assured by adjusting the time integration step.

With an adjustable parameterization factor, the DSP also provides isotropic eddy diffusion rates, K, which are taken to be independent of latitude and season. The increase of K with height, corresponding to the increasing GW momentum source (per mass), is a natural property of the model and is essential to simulate the QBO and SAO. In the mesosphere, the height dependence of K proves to be important for the tides and planetary waves. The GW generated heating rates are not accounted for in the model.

III. Diurnal Tides

It is well established that the diurnal tide in the mesosphere is dominated by the propagating mode that peaks at low latitudes. We then show with Figure 1 a contour plot of the computed meridional wind oscillations for different zonal wave numbers at 18° latitude (Gaussian point). Generated by the classical migrating solar excitation sources, the westward migrating tide is expected to dominate for m = 1, and this is reflected in Figure 1a. The shown oscillations, however, also contain the smaller eastward migrating tide (also called "non-migrating tide" because it does not migrate with the Sun), and planetary waves. With identical contour intervals, for comparison, we show in (b) the oscillations for m = 0, and in (c) those for m = 0, 2, 3, 4 combined, which reveal also diurnal variations. In these latter two cases, the diurnal variations are not generated by specified tidal excitation sources of any other kind. These variations are solely generated internally through dynamical interactions. With Figure 1d we then present the computed variations from all the zonal wave numbers retained in the model, m = 0 to 4. The differences are relatively large between Figure 1d and Figure 1a where the oscillations are dominated by the migrating tide for m = 1. As mentioned, the oscillations shown here contain also planetary wave signatures.

To provide a broad overview of the diurnal tides generated in the NSM, i.e., migrating and non-migrating but without planetary waves, we present in Figure 2 the computed amplitudes for the meridional winds with a period of 1 day (24 hours) for zonal wave numbers m = 0 to 4, delineating the eastward and westward propagating components. The tidal oscillations were extracted from a time span of two months (24 to 26 months) leading into the 3rd computer year and the Sun in the southern hemisphere. With a running window of 4 days, a Fourier analysis was carried out, and the largest amplitudes are plotted versus altitude. To reveal more clearly

the amplitude patterns, the lowest 50% of the contours are suppressed. The maximum values are stated in the lower left corner of each panel.

The computed wind amplitudes in Figure 2 show, as expected, that the westward (dashed) propagating component dominates for wave number m = 1 (with a maximum value of 83 m/s that developed near the time of 26 months). It peaks at low latitudes, with significant differences between the northern winter and southern hemispheres. By comparison, the eastward (solid) propagating component (29 m/s maximum) is small and does not appear in the chosen contour intervals. As pointed out earlier, this eastward propagating tide is not generated in the model explicitly by a prescribed source; and the same is true for all the other tidal components in Figure 2 including the one for m = 0 (58 m/s maximum). For the zonal wind amplitudes (somewhat smaller and not shown) the relative differences between wave numbers are similar to those for the meridional winds. With the horizontal Coriolis force vanishing at the equator, however, the computed zonal winds for m = 0 essentially vanish there. (The smaller vertical Coriolis force is accounted for in the NSM.)

To provide some details about the dominant tidal components for m = 1, we present in Figure 3 the computed meridional wind amplitudes at 100 km during the first two model years, delineating the total (eastward and westward) tide (a), and its westward (b) as well as eastward (c) components. This reveals the characteristic semiannual variation with maxima near equinox, which requires some time to fully develop during the second half of the year (and beyond that). As was evident in our earlier model results (Mayr et al., 2001a) for the total m = 1 diurnal tide (a), the large amplitude modulations are a signature of planetary wave (PW) interaction. The results shown here reveal that this PW modulation primarily affects the eastward propagating tide (c).

Addressing the relatively large m = 0 tide generated in the NSM, we present in Figure 4a the amplitude modulations (computed with a 3 day window) at 100 km for the two model years commensurate with Figure 3. This reveals temporal variations in particular during the first year that resemble those for the eastward propagating tide (Figure 3c). After the initial increase that produces a peak around 2 months, the amplitude decreases and then grows again to reach large maxima around 7 and 9 months. For comparison, we also present the computed m = 1 planetary waves (PWs) at 100 km for the meridional (b) and zonal (c) winds, which show a similar pattern. After the initial 2.5 months, the PW amplitudes decrease and then increase

again to reach peak values between 6.5 and 10 months – indicating that PWs interactions are the cause for this m = 0 non-migrating tide in the NSM.

That PWs indeed are the cause for the non-migrating tides is seen from the results of a numerical experiment reproduced in Figures 5 and 6, for which we selectively turned off the solar heating in m = 0 but retained the migrating tidal excitation source. While the amplitudes for the total m = 1 diurnal tide (Figure 5a) and the westward propagating tide (b) are comparable in magnitudes to those in Figures 3a and 3b respectively, the eastward propagating component (5c) is negligibly small. In this case, apparently, instabilities do not develop to generate PWs, as is seen from the small amplitudes in Figures 6b and 6c after the initial start-up noise (note the differences in the scales relative to Figures 4b and 4c). As a result, the m = 0 tide (Figure 6a) is also small, especially during the second half of the first model year and beyond that. As Talaat and Lieberman (1999) proposed, the non-migrating m = 0 tide is generated in our model by non-linear interactions that involve PWs.

To reveal the seasonal variations of non-migrating tides, we present in Figures 7 and 8 for m = 1 and 0 respectively contour plots of the computed zonal and meridional winds at 100 km. The eastward and westward tides with a period of 1 day (24 hours) are delineated, covering 2 model years (24 to 48 months). As expected, the most persistent seasonal variations appear in the westward propagating tides in Figure 7b and 7d, with the amplitude maxima occurring around equinox as observed. Consistent with the PW mechanism, the non-migrating tides appear intermittently as Figure 3 already had shown. The eastward propagating tide for the zonal winds at low latitudes (Figure 7a) tend to be largest in winter and during equinox and decidedly weaker in summer. There is a tendency for the meridional winds, which peak at the equator, to be larger during equinox. The seasonal variations of the diurnal tide for m = 0 (Figure 8) reveal similar trends. The zonal winds at low latitudes peak in winter and during equinox, and the meridional winds peak at the equator (as seen also in Figure 2), and their latitudinal extent tends to broaden around equinox.

Corresponding to the zonal and meridional winds shown above (Figure 7), we present in Figures 9 the seasonal variations of the computed temperature perturbations. For the dominant m = 1 westward propagating tide (Figure 9b), as expected, the temperatures peak at the equator and during equinox. The eastward propagating temperature tide (Figure 9a) tends to straddle the equator, and the amplitudes are generally larger around equinox. For m = 0, the diurnal

temperature tide is presented in Figure 10b along with the meridional winds (a). The temperature perturbations again tend to straddle the equator, and the meridional winds peak at the equator. This is qualitatively consistent with pressure driven winds across the equator that in turn cause dynamical heating and cooling at low latitudes away from the equator.

IV. Semi-Diurnal Tides

Analogous to Figure 2, we present in Figure 11 the height and latitude variations of the semi-diurnal tides in the meridional winds for the time span from 24 to 26 months. The westward migrating tide at m = 2 dominates, but the non-migrating tides at m = 0 and m = 1 in particular are also large. The tidal components for m = 3 and 4 are significant as well.

As Figure 11c shows, the dominant migrating semi-diurnal tide peaks at mid to high latitudes. Analogous to Figure 3, we thus present in Figure 12 the computed meridional wind amplitudes at 100 km for 62° latitude, delineating again the total tide (a) and its westward (b) and eastward (c) components. This shows the characteristic seasonal variation with maxima during summer and winter months. An analysis of earlier model results demonstrated that these variations are in part caused by non-linear coupling with the diurnal tide, which was attributed to GW filtering (Mayr et al., 2001a). As is the case for the diurnal tide (Figure 3), the amplitude modulations appear to be generated by planetary wave (PW) interaction, which is particularly effective for the much weaker eastward propagating component (Figure 12c).

The m = 0 semi-diurnal tide grows in amplitude at least up to 110 km (Figure 11a), consistent with the westward migrating tide (Figure 11c) that is involved to generate it. Analogous to Figure 4, we present in Figure 13a for first two model years the seasonal variations of the m = 0 semi-diurnal tide at 110 km. During the first year, the variations resemble those seen in Figure 4. After the first 2 months, the amplitude decreases and then grows again to reach a large maximum at around 8 months. As suggested by Talaat and Liberman (1999) for the diurnal tide, PW interactions can generate such a tidal component, and in the case of the semi-diurnal tide the waves need to be associated with m = 2. For comparison, we thus present the computed m = 2 PWs at 110 km for the meridional winds (Figure 13b). This shows then that the temporal variations of the stronger PWs (Figure 13b) correlate with the patterns in the m = 0 tide (Figure 13a). As was demonstrated for the diurnal tide, PWs indeed are the cause for the m = 0 non-migrating semi-diurnal tide. When we turn

off the solar heating for m = 0, the PWs (Figure 13d) disappear, and commensurate with that, the m = 0 tide then is also small (Figure 13c).

In Figure 14 we show the computed seasonal variations of the zonal and meridional winds for the m = 2 semi-diurnal tide at 100 km. The dominant westward propagating tide peaks in the winter hemisphere, and the same tends to be true for the eastward propagating tide except that its amplitudes are much smaller as seen from the numerical values of the maximum amplitudes shown in the left bottom corner of each panel. For m = 0 (not shown), the wind amplitudes at 100 km are also largest in the winter hemisphere at high latitudes.

Analogous to Figure 14, we present with Figure 15 the corresponding temperature perturbations that reveal again systematic seasonal variations. In the dominant westward tide (b), the largest amplitudes tend to occur in the winter hemisphere, but the somewhat weaker peaks in summer occur over longer time span. The amplitudes of the eastward propagating tide (a) are largest during the winter months and then extend to low latitudes.

As seen in Figure 14, the dominant westward migrating semi-diurnal tide (m = 2) in the upper mesosphere peaks at latitudes around 60°. For obvious geometric reasons, this tide vanishes at the poles, as do all other oscillations for zonal wave numbers $m \neq 1$. In contrast, the dominant westward propagating diurnal tide, and oscillations with m = 1 in general, are unique in that they do not need to vanish at the poles but instead may attain large amplitudes there. Interactions between the semi-diurnal tide and the m = 1 PWs thus can become important at high latitudes, as Forbes et al. (1995) had proposed. This is shown in Figures 16, where we present the computed oscillations at high latitudes (77°) for m = 1 (a) and for the sum of all the wave numbers m = 0, 1, 2, 3, 4 (b). With identical contour intervals, the semi-diurnal variations at m = 1 (a) are shown to be comparable to those for the combined wave numbers (b) that include the dominant m = 2 westward propagating semi-diurnal tide.

In Figure 17 we then show for 84° N the m = 1 semi-diurnal tide (a) together with the PWs that are involved in generating it. Solutions are presented computed with and without the m = 0 solar heating. With that source, the PWs are strong (b) and are clearly correlated with the tide (a). Without the m = 0 source, the PWs are essentially not excited as seen in (d), and the m = 1 semidiurnal tide (c) then is also small.

Commensurate with the above wind fields, relatively large temperature perturbations are generated at 100 km as is shown in Figure 18. Like the eastward propagating m = 2 tide in

Figure 15a, the largest amplitudes occur during winter months where the migrating semi-diurnal tide (Figure 15b) is strongest.

As a signature of solar forcing, our model produces systematic seasonal variations not only in the migrating tides but in the non-migrating diurnal and semi-diurnal tides as well. To provide a more thorough understanding will require that we relate these variations to the seasonal variability of PWs and migrating tides, which goes beyond the scope of this paper.

V. Discussion and Conclusion

We have shown here for the diurnal and semi-diurnal tides, that non-migrating components with relatively large amplitudes are generated in the NSM at altitudes above 80 km. The evidence presented indicates that the non-migrating tides are caused by dynamical interactions between the migrating tides and PWs generated in the model through instabilities. This process was proposed by Forbes et al. (1995) for the m = 1 semidiurnal tide at polar latitudes and by Talaat and Lieberman (1999) for the m = 0 diurnal tide. Non-linear interactions between long period planetary waves for m = 1 and 2, $\exp(i\Omega t \pm im\varphi)$, and the westward propagating tides, $\exp(im\omega t - im\varphi)$, would yield with $\Omega << \omega$ approximately $\approx \exp(im\omega t)$ for m = 0, and $\approx \exp(i\omega t - 2im\varphi)$, each modulated by the PWs. We have seen from Figures 4 and 6 for the diurnal tide and from Figure 13 for the semi-diurnal tide that this indeed appears to be the explanation. The process was also shown to operate for the large m = 1 semi-diurnal tide as seen from Figure 17. A limited inspection of our model results in fact indicates that PWs are involved in generating the non-migrating tides in general.

The NSM solves the non-linear Navier Stokes equations and thus can account for the above-discussed non-linear coupling. There are a number of non-linear processes that can be in play such as advection and adiabatic heating, and they still need to be investigated.

Our model also accounts for GW processes and in particular for the filtering of GWs, which can produce non-linear interactions as we had argued earlier (Mayr et al., 1999, 2001, 2002). Gravity wave filtering is a natural candidate for generating non-linear interactions between the QBO and SAO to produce inter-seasonal variations in the upper mesosphere, between the QBO and the AO (annual oscillation) to produce quasi-decadal oscillations, and between the diurnal and semidiurnal tides. In the present case, upward propagating GWs may encounter a PW and amplify it (Mayr et al., 2001b). This amplification occurs at the expense of the GW momentum

flux in a particular direction, which in turn decreases the flux in that direction. The GW flux, thus modified by the PW, then encounters the tide and amplifies it (Mayr et al., 2001a). The PW modulation in the GWs is thereby transferred to the tide, which represents a non-linear interaction. Such a process is likely to be less important at lower altitudes where the filtering would not cut as deeply into the momentum flux. But at higher altitudes, this process becomes increasingly more important as the remaining GW momentum gets depleted by absorption and by the accompanying filtering. Apart from the fact that the tides and PWs tend to grow with altitude, the non-linear process of GW filtering on its own may become increasingly more important at higher altitudes. All this combined may help to explain, in part, why the non-migrating tides become so important in the upper mesosphere as our model results indicate.

In conclusion, we present a schematic with Figure 19 that summarizes the results from our modeling study and outlines our present understanding of the processes that are involved in generating the non-migrating tides in the NSM. The model is driven exclusively by solar heating, which is the source for the westward migrating diurnal and semi-diurnal tides and, separately, for the mean zonal circulation. For simplicity, a steady source of parameterized small-scale gravity waves (GW) is imposed, which is independent of latitude and season. As outlined in Figure 19 and discussed in the literature, the GWs produce temperature and wind reversals in the upper mesosphere (1) and affect significantly the tides (2) and planetary waves (3). Following Forbes et al. (1995) and Talaat and Lieberman (1999), we showed in the present paper that non-linear coupling between migrating tides and planetary waves (PW) can produce non-migrating tides in the upper mesosphere, having magnitudes comparable to those observed. By artificially turning off the solar heating for the mean zonal circulation, the PWs were suppressed and so were the non-migrating tides. Filtered by the mean zonal circulation, the PWs are apparently generated in the model by instabilities, which still need to be explored.

As Figure 19 illustrates, GWs contribute in several important ways to the non-migrating tides by influencing significantly their building blocks, i.e., the tides and PWs. Without GWs, the mean zonal circulation would be significantly different, which in turn would affect the instabilities that generate the PWs in the NSM. In addition, the tides and PWs are amplified by the GWs. Thus it is difficult to completely isolate the role GWs can play as a non-linear agent in coupling the tides and PWs (5). Notwithstanding this difficulty, we have carried out

numerical experiments that do suggest this process is important, and we present our findings in the accompanying paper (Part II).

Another subject to be discussed will deal with the importance of tropospheric zonally symmetric (m = 0) cumulus heating that generates the zonal jest near the tropopause, which is a source of planetary waves that in turn contribute significantly to the non-migrating tides. In a separate paper (Talaat et al., 2003), we shall discuss the non-migrating pseudo tides that are generated in the model without the explicit excitation of the solar driven westward migrating tides.

References

Akmaev, R. A., Simulation of large-scale dynamics in the mesosphere and lower thermosphere with the Doppler-spread parameterization of gravity waves: 2. Eddy mixing and the diurnal tide, *J. Geophys. Res.*, **106**, 1205, 2001a

Akmaev, R. A., Simulation of large-scale dynamics in the mesosphere and lower thermosphere with the Doppler-spread parameterization of gravity waves: 1. Implementation and zonal mean climatologies, *J. Geophys. Res.*, **106**, 1193, 2001b

Avery, S. K., R. A. Vincent, A. Phillips, A. H. Manson, and G. R. Fraser, High latitude tidal behavior in the mesosphere and lower thermosphere, *J. Atm. Terr. Phys.*, **51**, 595, 1989

Burrage M. D., M. E. Hagan, W. R. Skinner, D. L. Wu, and P. B. Hays, Long-term variability in the solar diurnal tide observed by HRDI and simulated by the GSWM, *Geophys. Res. Lett.*, **22**, 2641, 1995a

Burrage M. D., D. L. Wu, W. R. Skinner, D. A. Ortland, and P. B. Hays, Latitude and seasonal dependence of the semidiurnal tide observed by the high-resolution Doppler imager, *J. Geophys. Res.*, **100**, 11313, 1995b

Chan, K. L., H. G. Mayr, J. G. Mengel, and I. Harris, A 'stratified' spectral model for stable and convective atmospheres, *J. Comp. Phys.*, **113**, 165, 1994a

Chan, K. L., H. G. Mayr, J. G. Mengel, and I. Harris, A spectral approach for studying middle and upper atmospheric phenomena, *J. Atmos. Terr. Phys.*, **56**, 1399, 1994b

Chapman, S., and R. S. Lindzen, *Atmospheric Tides*, D. Reidel, Hingham, MA, 1970

Forbes, J. M., and H. B. Garrett, Thermal excitation of atmospheric tides due to insolation absorption by O_3 and H_2O, *Geophys. Res. Lett.*, **5**, 1013, 1978

Forbes, J. M, and M. E. Hagan, Diurnal propagating tides in the presence of mean winds and dissipation: a numerical investigation, *Planet. Space Sci.*, **36**, 579, 1988

Forbes, J. M., and F. Vial, Monthly simulations of solar semidiurnal tide in the mesosphere and lower thermosphere, *J. Atm. Terr. Phys.*, **51**, 649, 1989

Forbes, J. M, J. Gu, and S. Miyahara, On the interactions between gravity waves and the diurnal propagating tide, *Planet. Space Sci.*, **39**, 1249, 1991

Forbes, J. M., Tidal and planetary waves, *Geophysical Monograph* **87**, 67, 1995

Fritts, D. C., Gravity wave-tidal interactions in the middle atmosphere: observations and theory, *Geophysical Monograph* **87**, 89, 1995a

Fritts, D. C., Gravity wave forcing and effects in the mesosphere and lower thermosphere, *Geophysical Monograph* **87**, 121, 1995b

Geller, M. A., V. A. Yudin, B. V. Khattatov, and M. E. Hagan, Modeling the diurnal tide with dissipation derived from UARS/HRDI measurements, *Ann. Geophys.*, **15**, 1198, 1997

Hagan, M. E. and R. G. Roble, Modeling diurnal tidal variability with the National Center for Atmospheric Research thermosphere-ionosphere-mesosphere-electrodynamics general circulation model, *J. Geophys. Res.*, **106**, 24,869-24,882, 2001

Hagan, M. E., Comparative effects of migrating solar sources on tidal signatures in the middle and upper atmosphere, *J. Geophys. Res.*, **101**, 21213, 1996

Hagan, M. E., J. M. Forbes, and F. Vial, On modeling migrating solar tides, *Geophys. Res. Lett.*, **22**, 893, 1995

Hays, P. B. et al. The high-resolution Doppler imager on the Upper Atmosphere Research Satellite, *J. Geophys. Res.*, **98**, 10,713, 1993

Hays, P. B., D. L. Wu, and the HRDI science team, Observations of the diurnal tide from space, *J. Atmos. Sci.*, **51**, 3077, 1994

Hines, C. O., Doppler-spread parameterization of gravity-wave momentum deposition in the middle atmosphere, 1, Basic formulation, *J. Atmos. Solar Terr. Phys.*, **59**, 371, 1997a

Hines, C. O., Doppler-spread parameterization of gravity-wave momentum deposition in the middle atmosphere, 2, Broad and quasi monochromatic spectra, and implementation, *J. Atmos. Solar Terr. Phys.*, **59**, 387, 1997b

Jacobi, C. et al., Mesopause region semidiurnal tide over Europe as seen from ground-based wind measurements, *Adv. Space Res.*, **24**, 1545, 1999

Lindzen R. S., Turbulence and stress due to gravity wave and tidal breakdown, *J. Geophys., Res.*, **86**, 9707, 1981

Lindzen, R. S., and S. Hong, Effects of mean winds and horizontal temperature gradients on solar and lunar semidiurnal tides in the atmosphere, *J. Atm. Sci.*, **31**, 1421, 1974

Mancini, E., N. A. McFarlane, and C. McLandress, Impact of the Doppler spread parameterization the simulation of the middle atmosphere circulation using the MA/ECHAM4 general circulation model, *J. Geophys. Res.*, **102**, 25,751, 1997

Manson, A. H., C. E. Meek, H. Teitelbaum, F. Vial., R. Schminder, D. Kuerschner, M. J. Smith, G. J. Fraser, and R. R. Clark, Climatology of semi-diurnal and diurnal tides in the middle atmosphere (70-110 km) at middle latitudes (40-55^{o}), *J. Atm. Terr. Phys.*, **51**, 579, 1989

Mayr, H. G., J. G. Mengel, C. A. Reddy, K. L. Chan, and H. S. Porter, The role of gravity waves in maintaining the QBO and SAO at equatorial latitudes, *Adv. Space Res.*, 24, 1541, 1999

Mayr, H. G., J. G. Mengel, K. L. Chan, and H. S. Porter, Seasonal variations of the diurnal tide induced by gravity wave filtering, *Geophys. Res. Lett.*, **25**, 943, 1998

McLandress, C., G. G. Shepherd, and B. H. Solheim, Satellite observations of thermospheric tides: Results from the Wind Imaging Interferometer on UARS, *J. Geophys. Res.*, **101**, 4093, 1996

McLandress, C., Seasonal variability of the diurnal tide: Results from the Canadian Middle Atmosphere General Circulation Model, J. *Geophys. Res.*, **102**, 29747, 1997a

McLandress, C., Sensitivity studies using the Hines and Fritts gravity wave drag parameterization, *NATO ASI Series*, Vol. I 50, 245, 1997b

Mengel, J. G., Mayr, H. G., Chan, K. L., Hines, C. O., Reddy, C. A., Arnold, N. F., Porter, H. S., 1995. Equatorial oscillations in the middle atmosphere generated by small-scale gravity waves, *Geophys. Res. Lett.*, **22** , 3027

Miyahara, S., Y, Miyoshi, and K. Yamashita, Variations of migrating and nonmigrating atmospheric tides simulated by a middle atmosphere general circulation model, *Adv. Space Res.*, **24(11)**, 1549-1558, 1999.

Miyahara, S, Y. Toshida, and Y. Miyoshi, Dynamical coupling between the lower and upper atmosphere by tides and gravity waves, *J. Atm. Terr. Phys.*, **55**, 1039, 1993

Miyahara, S., and J. M. Forbes, Interactions between gravity waves and the diurnal tide in the mesosphere and lower thermosphere, *J. Meteor. Soc. Japan*, **69**, 523, 1991

Norton, W. A., and J. Thuburn, The two-day wave in a middle atmosphere GCM, *Geophys. Res. Lett.*, **23**, 2113, 1996

Norton, W. A., and J. Thuburn, Sensitivity of mesospheric mean flow, planetary waves and tides to strength of gravity wave drag, J. *Geophys. Res.*, **104**, 30,897, 1999

Plumb, R. A., Baroclinic instability of the summer mesosphere: A mechanism for the quasi-2-day wave?, *J. Atmos. Sci.*, **40**, 262, 1983

Shepherd, G. G., et al., WINDII, the Wind Imager Interferometer on the Upper Atmosphere Research Satellite, *J. Geophys. Res.*, **98**, 10,7725, 1993

Talaat, E. R., and R. Lieberman, Nonmigrating diurnal tides in mesospheric and lower thermospheric winds and temperatures *J. Atmos. Sci.*, **56**, 4073, 1999

Strobel, D. F., Parameterization of atmospheric heating rate from 15 to 120 km due to O2 and O3 absorption of solar radiation, *J. Geophys. Res.*, **83**, 7963, 1978

Teitelbaum, H. and F. Vial, On tidal variability induced by nonlinear interaction with planetary waves, *J. Geophys. Res.*, **96**, 14,169-14,178, 1991

Walterscheid, R. L., G. G. Sivjee. G. Schubert, and R. M. Hamwey, Large amplitude semidiurnal temperature variations in the polar mesopause: evidence of pseudotide, *Nature*, **324**, 1986

Vial, F., and J. M. Forbes, Recent progress in tidal modeling, *J. Atm. Terr. Phys.*, **51**, 663, 1989

Vincent, R. A., T. Tsuda, and S. Kato, Asymmetries in mesospheric tidal structure, *J. Atm. Terr. Phys.*, **51**, 609, 1989

Volland, H., *Atmospheric Tidal and Planetary Waves*, Kluwer Academic Publ., Boston, MA, 1988

Yudin, V. A., B. V. Khattatov, M. A. Geller, et al.. Thermal tides and studies to tune the mechanistic tidal model using UARS observations, *Ann. Geophys.*, **15**, 1205, 1997

Figure Captions

Figure 1: Contour plots of computed temporal variations of the meridional winds at 18° latitude for m = 1 (a) that includes the dominant westward migrating diurnal tide (period of 1 day, or 24 hours), for m = 0 (b), for the sum m = 0, 2, 3, 4 (c) that does not include the

westward migrating tide, and m = 0, 1, 2, 3, 4 (c) that contains all the wave numbers retained in the model. Note that no filtering has been applied so that besides the tides planetary waves are also included. In all four panels, the diurnal tide dominates. But the differences clearly reveal that the non-migrating tides, exclusively present in (b) and (c), are also relatively large. The model presented here accounts for the classical westward migrating excitation sources only. The non-migrating tides are thus solely generated by dynamical interactions.

Figure 2: For a period after solstice (24 to 26 months), with the Sun in the southern hemisphere, we show for m = 0 to 4 the computed amplitudes of the meridional winds for the fundamental diurnal tide with period of 1 day (24 hours). The eastward and westward propagating components are respectively identified with solid and dashed contour lines. The contours were truncated below 50% of the maximum amplitudes to eliminate cluttering, but the maximum amplitudes are indicated in each panel for both eastward and westward propagating tides.

Figure 3: Computed amplitudes of the zonal wave number m = 1 diurnal tide at 100 km altitude for the first two model years, delineating the total (eastward and westward) tide (a) and its westward (b) and eastward (c) components. Note the large planetary wave (PW) modulation of the eastward component (c), which appears also in the combined tidal oscillation (a) but is much weaker in the dominant westward component (b).

Figure 4: Temporal variations for the amplitudes of the m = 0 tide during the first two model years at 100 km (a), and the computed meridional (b) and zonal (c) winds of the m = 1 PWs at this altitude. Note the correlations in the temporal variations of the amplitudes for the PWs (b, c) with the m = 0 tide (a) and with the eastward tide in Figure 3c, in particular during the first model year.

Figure 5: Same as Figure 3 but computed without the zonal mean (m = 0) solar heating, which generates the seasonally varying mid latitude zonal jets and temperature variations that reverse with latitude above about 70 km. The tides generated in this case are comparable in amplitude with those shown in Figure 2, but the eastward component (c) and the PW modulations are negligible.

Figure 6: Same as Figure 4 but without the m = 0 heat source as in Figure 5. Note the small PW amplitudes (b, c) for m = 1 (with scales different from those in Figure 4), and the corresponding small m = 0 tide (a). After the start-up noise during the first half model year, the

PWs and tide drastically decrease to attain small values that continue to remain small beyond the second model year.

Figure 7: Seasonal and latitudinal variations of the zonal and meridional winds at 100 km for the m = 1 diurnal tide delineated into eastward and westward components. As expected, the westward tide (b, d) dominates. While the zonal winds (b) reveal an annual cycle, with narrow amplitude peaks between winter and spring, the meridional wind amplitudes (c) peak near equinox. The eastward tide (a, c) is small by comparison as seen from the numerical values of amplitude maxima shown at the lower left corner of each panel. The zonal winds of this tidal component (a) peaks at low latitudes; and in the seasonal variations, the tidal activity is distinctly reduced during summer months. In contrast to that, the associated meridional winds (c) peak at the equator without revealing a distinct seasonal variation. The lower 50% of contours were suppressed in order to reveal the patterns more clearly.

Figure 8: Similar to Figure 7 but for the m = 0 diurnal tide. As in Figure 7, it shows that the zonal winds (a) for this component peak at low latitudes where the dominant westward migrating tide peaks, and the tidal activity is reduced during summer months. The meridional winds (b) peak at the equator as is also apparent from Figure 2.

Figure 9: Computed temperature perturbations for the eastward (a) and westward (b) propagating m = 1 diurnal tides. As expected, the amplitudes of the dominant westward migrating tide (b) peak at the equator near equinox. For the much weaker eastward component (a), the temperature perturbations are scattered and tend to straddle the equator.

Figure 10: Computed meridional winds (a) and temperature perturbations (b) for the m = 0 diurnal tide. The temperatures straddle the equator, which is consistent with the meridional winds that peak at the equator to cause dynamical heating and cooling at low latitudes.

Figure 11: Similar to Figure 2 but for the semi-diurnal tide (with 12 hour period). In this case, the dominant westward migrating tide is associated with m = 2 (c). Large non-migrating tides are generated for m = 0 (a) and m = 1 in particular (b).

Figure 12: Similar to Figure 3 but for the semi-diurnal tide at m = 2 and 62° latitude. Note the tidal variability of the eastward migrating tide (c), which is largest during winter months at this altitude.

Figure 13: Similar to Figure 4 but for the m = 0 semi-diurnal tide (a) and the m = 2 PWs (b) at 110 km and 62° latitude, which reveal correlations. For comparison, a solution is presented

for the tide (c) and PWs (d) without the m = 0 heat source. This demonstrates again that PWs are involved in generating the nonmigrating tide.

Figure 14: Similar to Figure 7 but for the semi-diurnal tide at tide at m = 2. It shows for the westward migrating tide that the zonal (a) and meridional (b) winds peak at around 62° latitude in the winter hemisphere. The eastward migrating components (a, c) are highly variable and small by comparison, but they peak in the winter hemisphere also.

Figure 15: Similar to Figure 9 but for the semi-diurnal tide at m = 2. The temperature perturbations of the dominant westward migrating tide (b) peak in winter, with a secondary maximum in summer, while the intermittent eastward propagating tide (a) develops mainly during winter months.

Figure 16: Analogous to Figure 1, contour plots of computed temporal variations in the meridional winds at 77° latitude for m = 1 (a) and for m = 0, 1, 2, 3, 4 (b) that contains all the wave numbers retained in the model. The dominant westward migrating semi-diurnal tide is associated with m = 2 (b). But the 12-hour periodicity is also apparent in m = 1 (a) where it represent a relatively large nonmigrating tide that extends into the polar region.

Figure 17: Temporal variations of amplitudes for the semi-diurnal m = 1 meridional winds at 84° (a), and the PWs for m = 1 (b) that are involved in generating this tide. For comparison a solution is shown without m = 0 heating, which yields tidal amplitudes (c) and PWs (d) that are negligibly small.

Figure 18: Seasonal variations of temperature perturbations for the m = 1 nonmigrating semi-diurnal tides, eastward (a) and westward (b), which tend to peak during winter months when the migrating tide is largest.

Figure 19: Schematic to illustrate the dynamical features and processes that produce non-migrating tides in the NSM. The model is driven by: (a) solar heating that generates the zonal mean (m = 0) circulation (and temperature variations) and the westward migrating tides, and (b) a gravity wave (GW) source independent of latitude and season. Planetary waves (PW) are generated solely by instabilities and filtering associated with the mean zonal circulation. Enumerated with items 1 to 4 and discussed in the literature, the GWs affect: (1) the zonal mean (m = 0) circulation and temperature variations, (2) the migrating tides, (3) the PWs , and (4) the equatorial oscillations (QBO, SAO). Gravity wave filtering contributes to the non-linear coupling between tides and PWs (item 5), which is discussed in a separate paper (Part II).

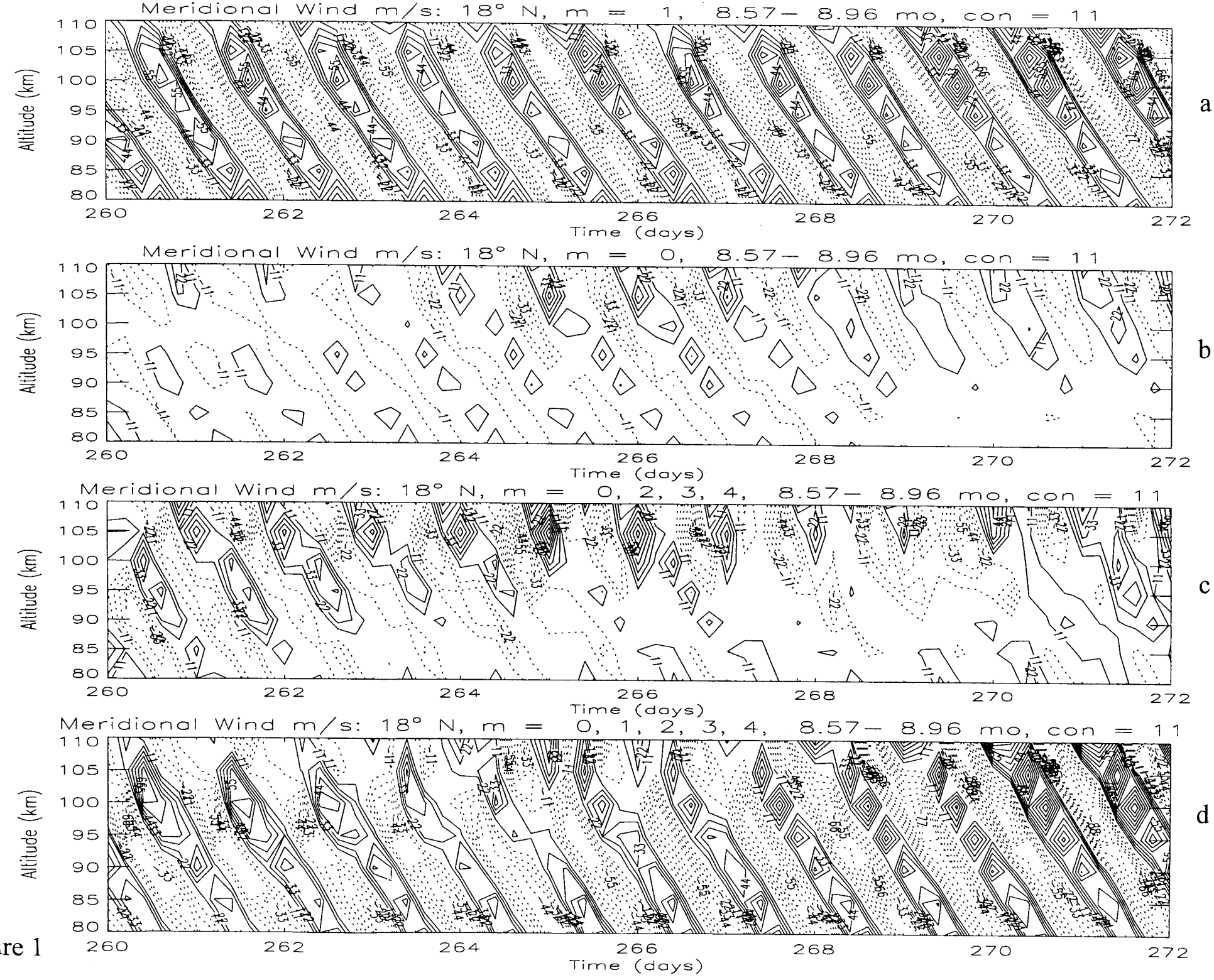
Meridional Wind m/s: 18° N, m = 1, 8.57– 8.96 mo, con = 11
Meridional Wind m/s: 18° N, m = 0, 8.57– 8.96 mo, con = 11
Meridional Wind m/s: 18° N, m = 0, 2, 3, 4, 8.57– 8.96 mo, con = 11
Meridional Wind m/s: 18° N, m = 0, 1, 2, 3, 4, 8.57– 8.96 mo, con = 11
Altitude (km)
110
105
100
95
90
85
80
260
262
264
266
268
270
272
Time (days)
a
b
c
d

Figure 1

Diurnal Tides (24 hour)

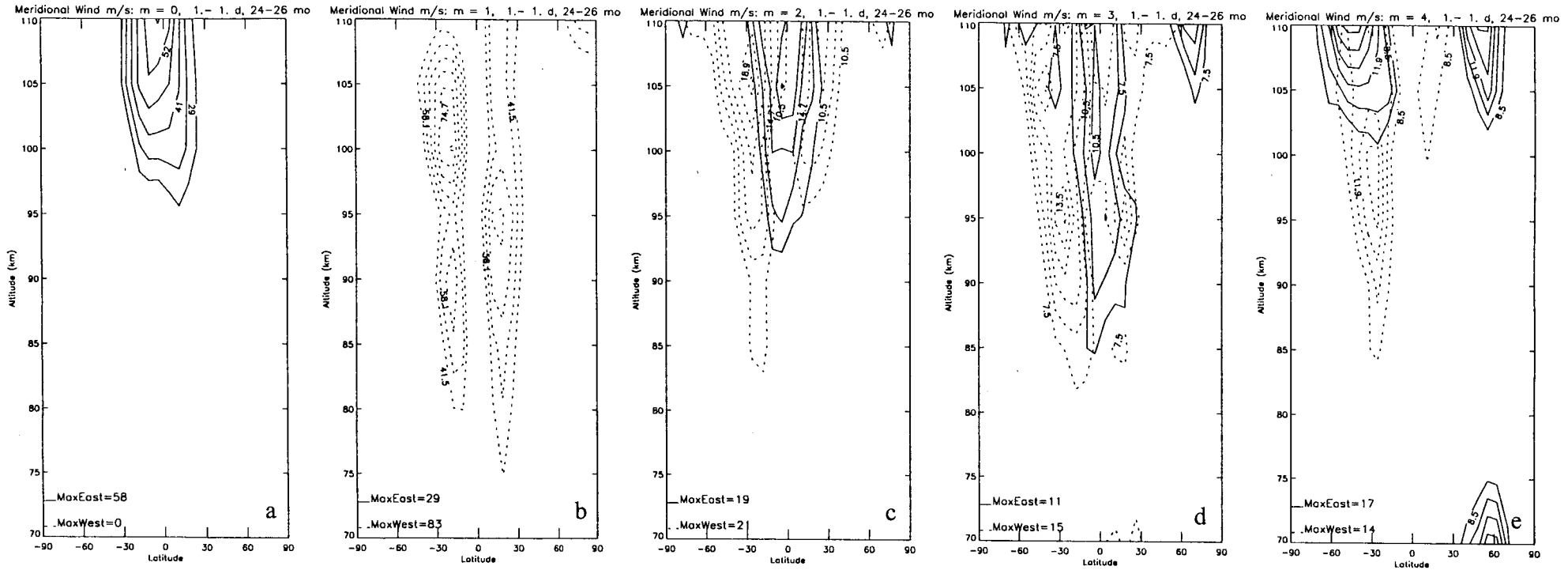

Figure 2

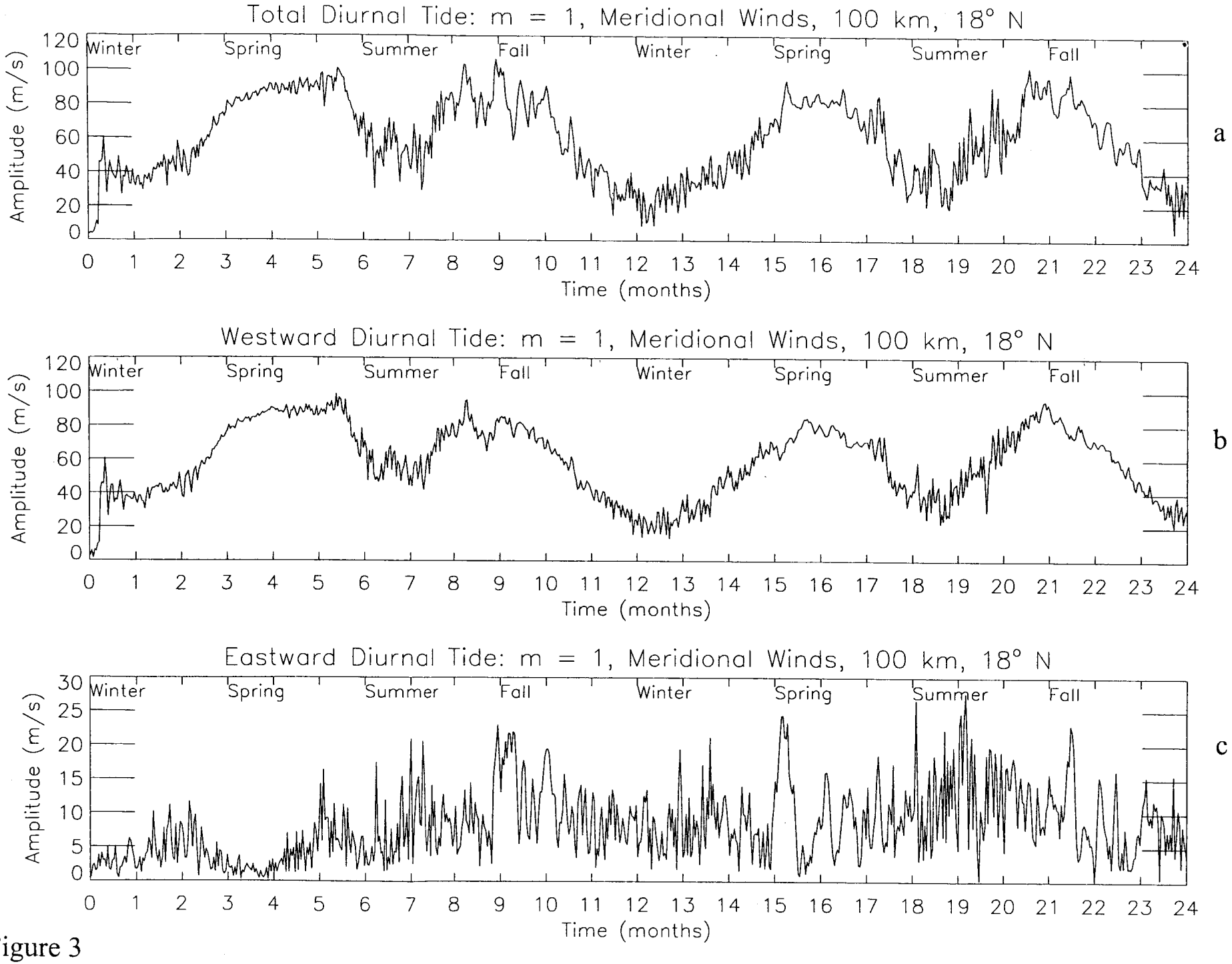
Total Diurnal Tide: m = 1, Meridional Winds, 100 km, 18° N
Westward Diurnal Tide: m = 1, Meridional Winds, 100 km, 18° N
Eastward Diurnal Tide: m = 1, Meridional Winds, 100 km, 18° N
Winter
Spring
Summer
Fall
Amplitude (m/s)
Time (months)
a
b
c

Figure 3

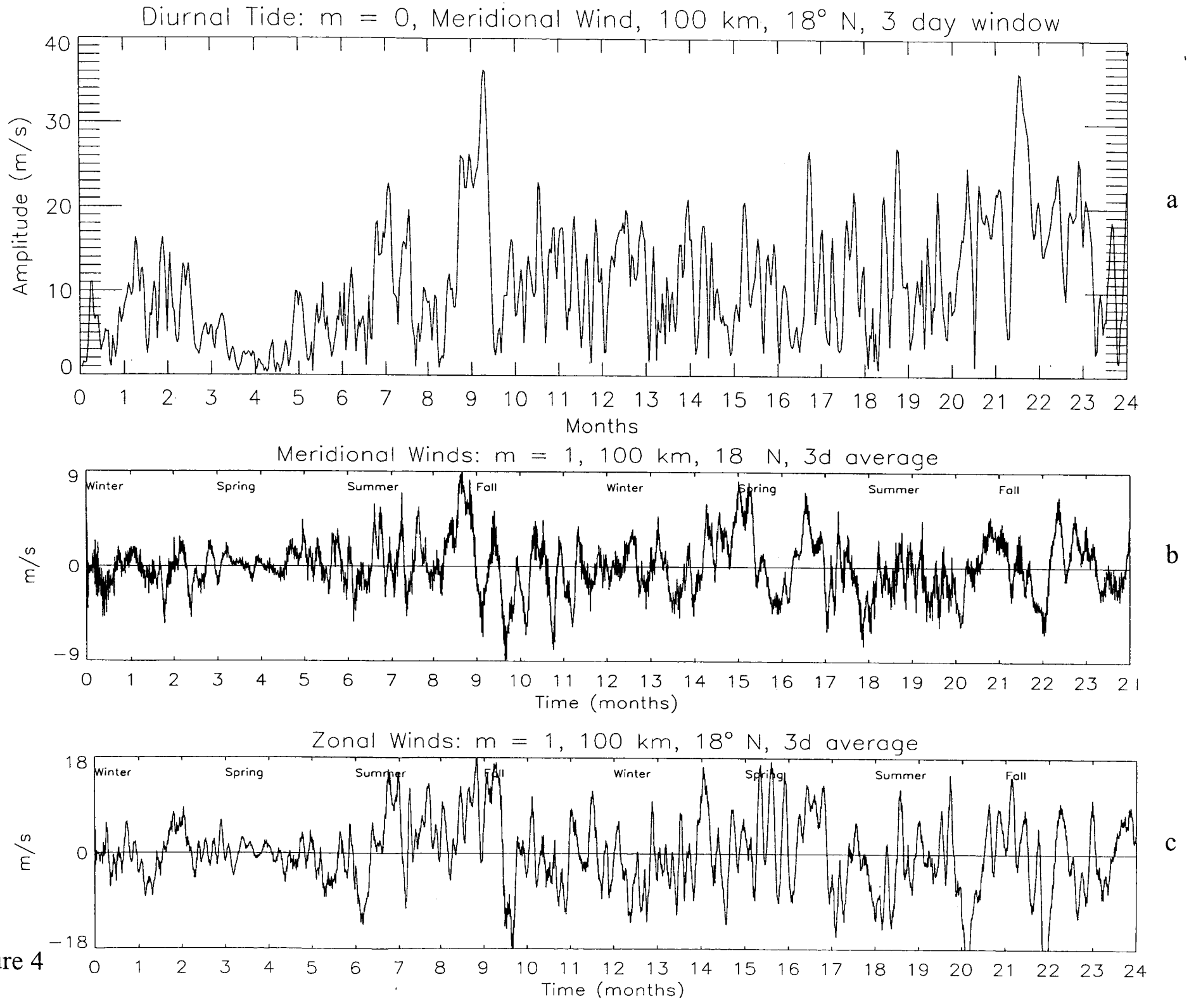
Diurnal Tide: m = 0, Meridional Wind, 100 km, 18° N, 3 day window
Amplitude (m/s)
Months
a
Meridional Winds: m = 1, 100 km, 18 N, 3d average
Winter
Spring
Summer
Fall
m/s
Time (months)
b
Zonal Winds: m = 1, 100 km, 18° N, 3d average
c

Figure 4

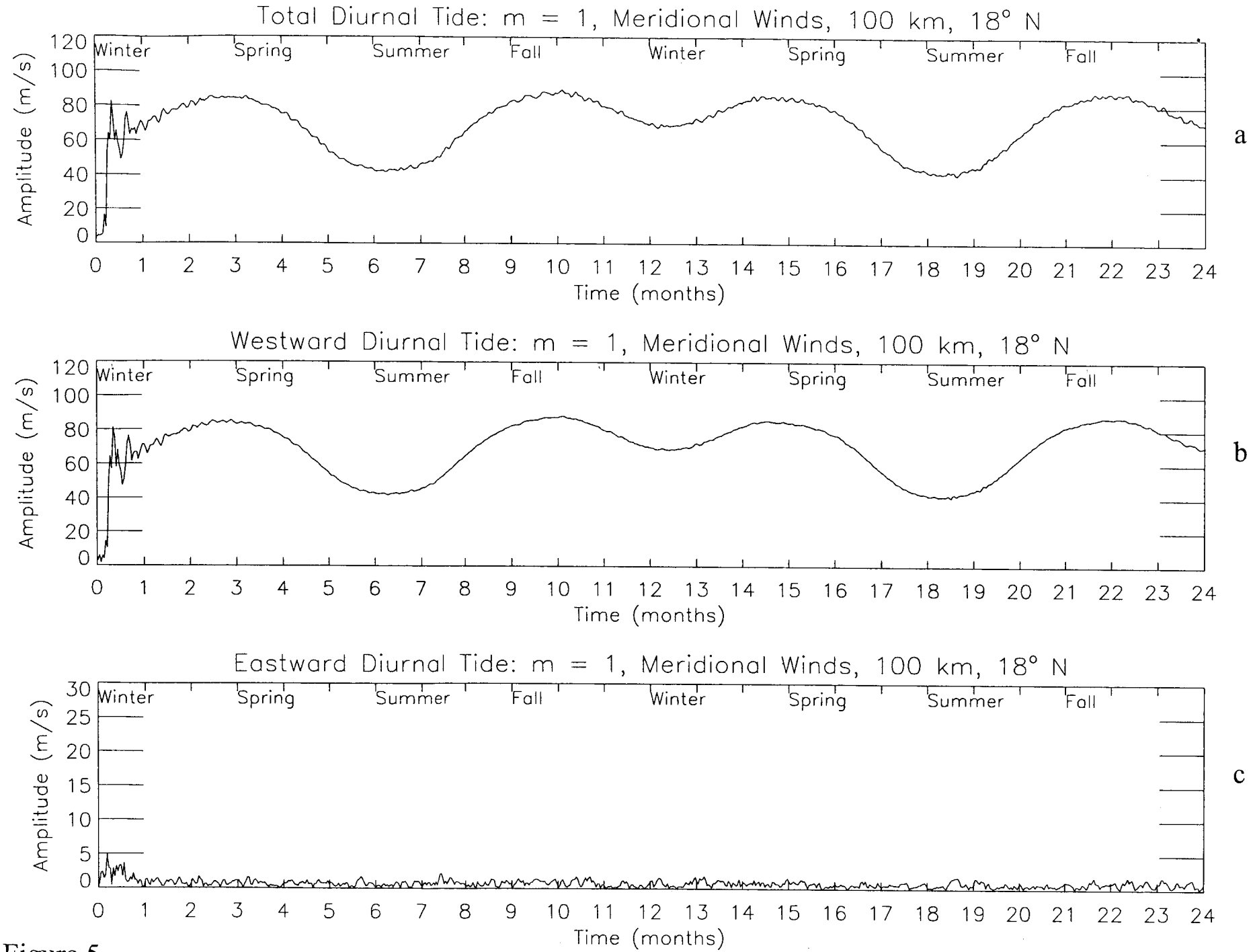
Total Diurnal Tide: m = 1, Meridional Winds, 100 km, 18° N
Amplitude (m/s)
120
100
80
60
40
20
0
Winter
Spring
Summer
Fall
Winter
Spring
Summer
Fall
0 1 2 3 4 5 6 7 8 9 10 11 12 13 14 15 16 17 18 19 20 21 22 23 24
Time (months)
a
Westward Diurnal Tide: m = 1, Meridional Winds, 100 km, 18° N
Amplitude (m/s)
120
100
80
60
40
20
0
Winter
Spring
Summer
Fall
Winter
Spring
Summer
Fall
0 1 2 3 4 5 6 7 8 9 10 11 12 13 14 15 16 17 18 19 20 21 22 23 24
Time (months)
b
Eastward Diurnal Tide: m = 1, Meridional Winds, 100 km, 18° N
Amplitude (m/s)
30
25
20
15
10
5
0
Winter
Spring
Summer
Fall
Winter
Spring
Summer
Fall
0 1 2 3 4 5 6 7 8 9 10 11 12 13 14 15 16 17 18 19 20 21 22 23 24
Time (months)
c

Figure 5

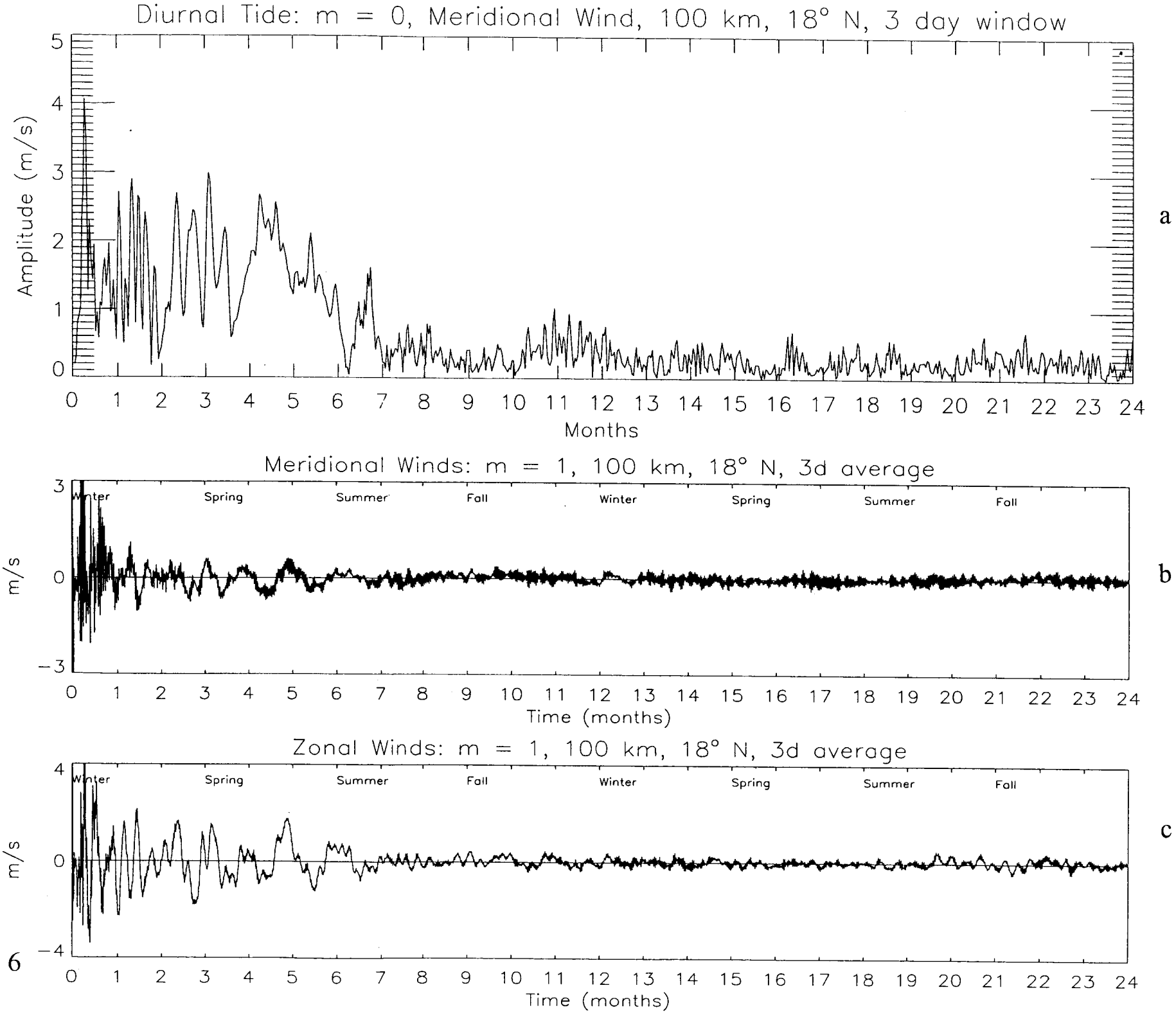
Diurnal Tide: m = 0, Meridional Wind, 100 km, 18° N, 3 day window
Amplitude (m/s)
Months
a
Meridional Winds: m = 1, 100 km, 18° N, 3d average
Winter
Spring
Summer
Fall
Winter
Spring
Summer
Fall
m/s
Time (months)
b
Zonal Winds: m = 1, 100 km, 18° N, 3d average
Winter
Spring
Summer
Fall
Winter
Spring
Summer
Fall
m/s
Time (months)
c

Figure 6

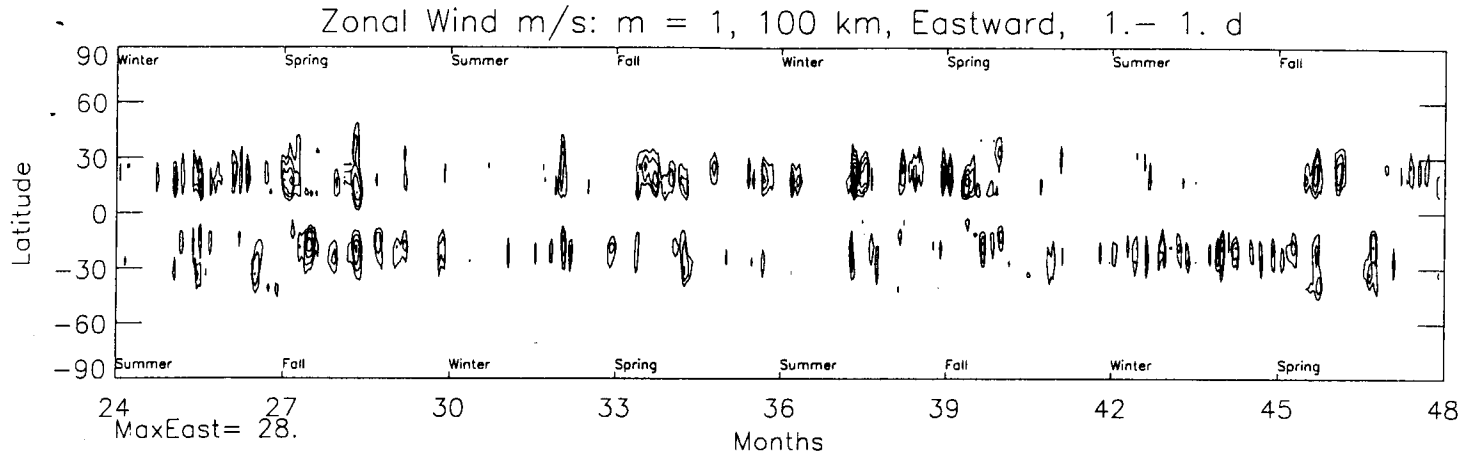

a

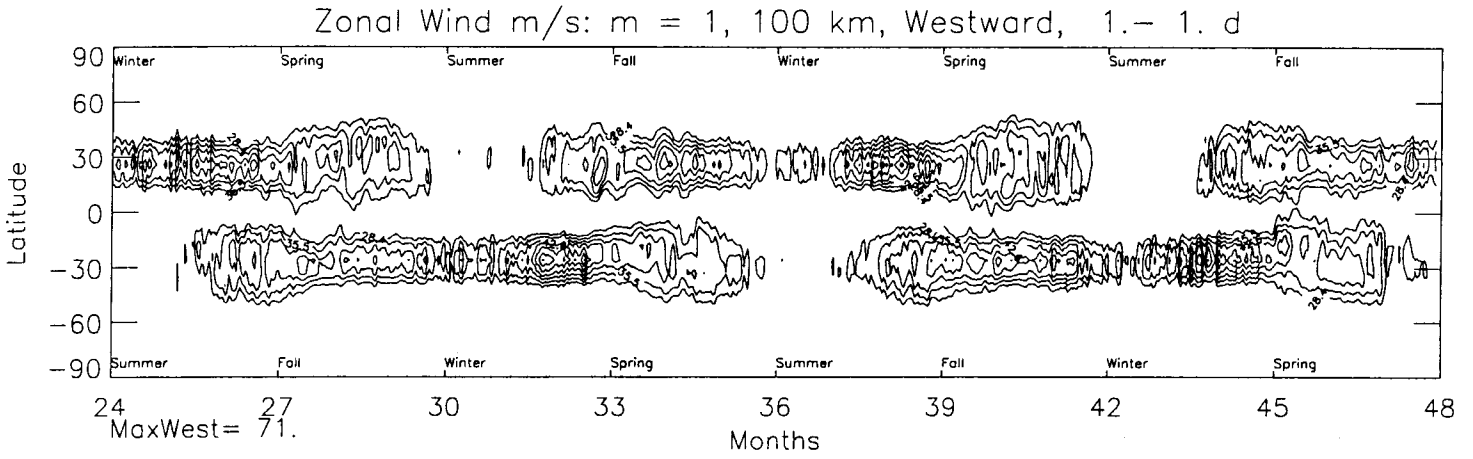

b

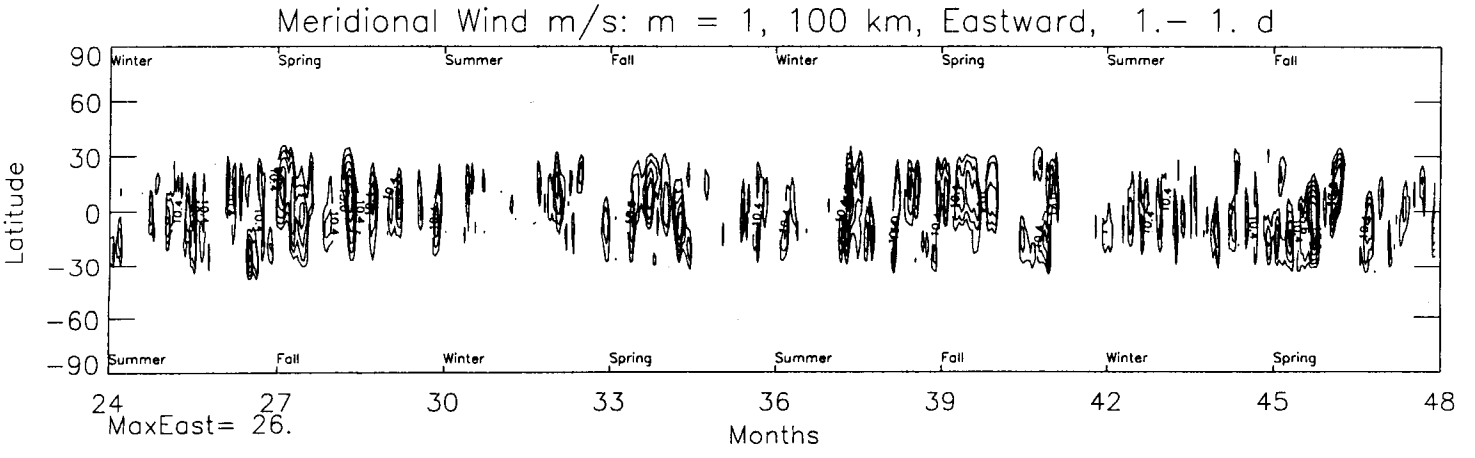

c

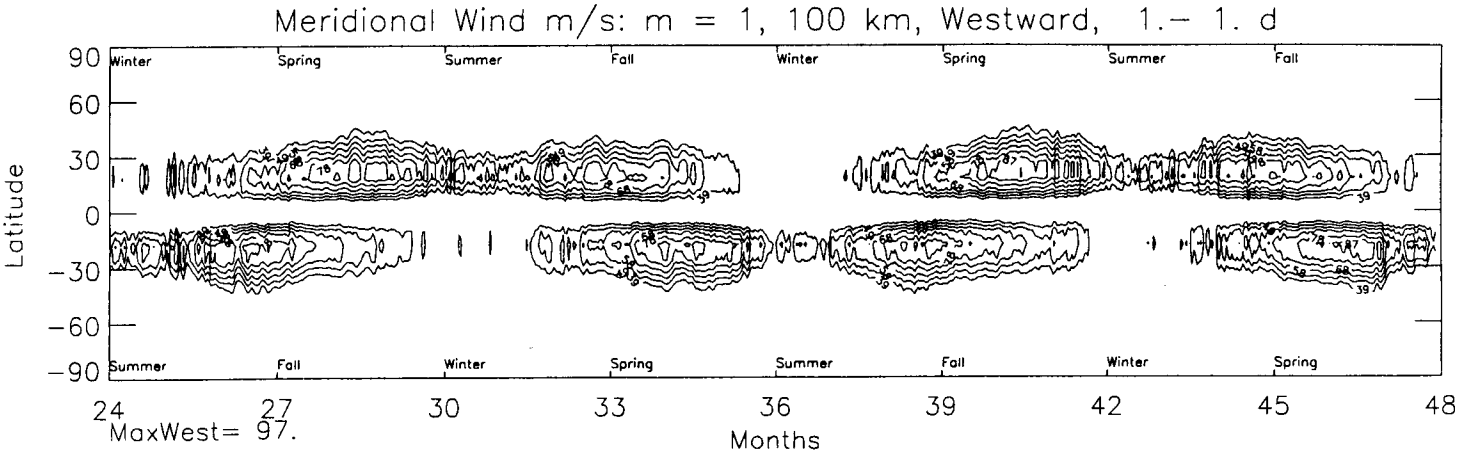

d

Figure 7

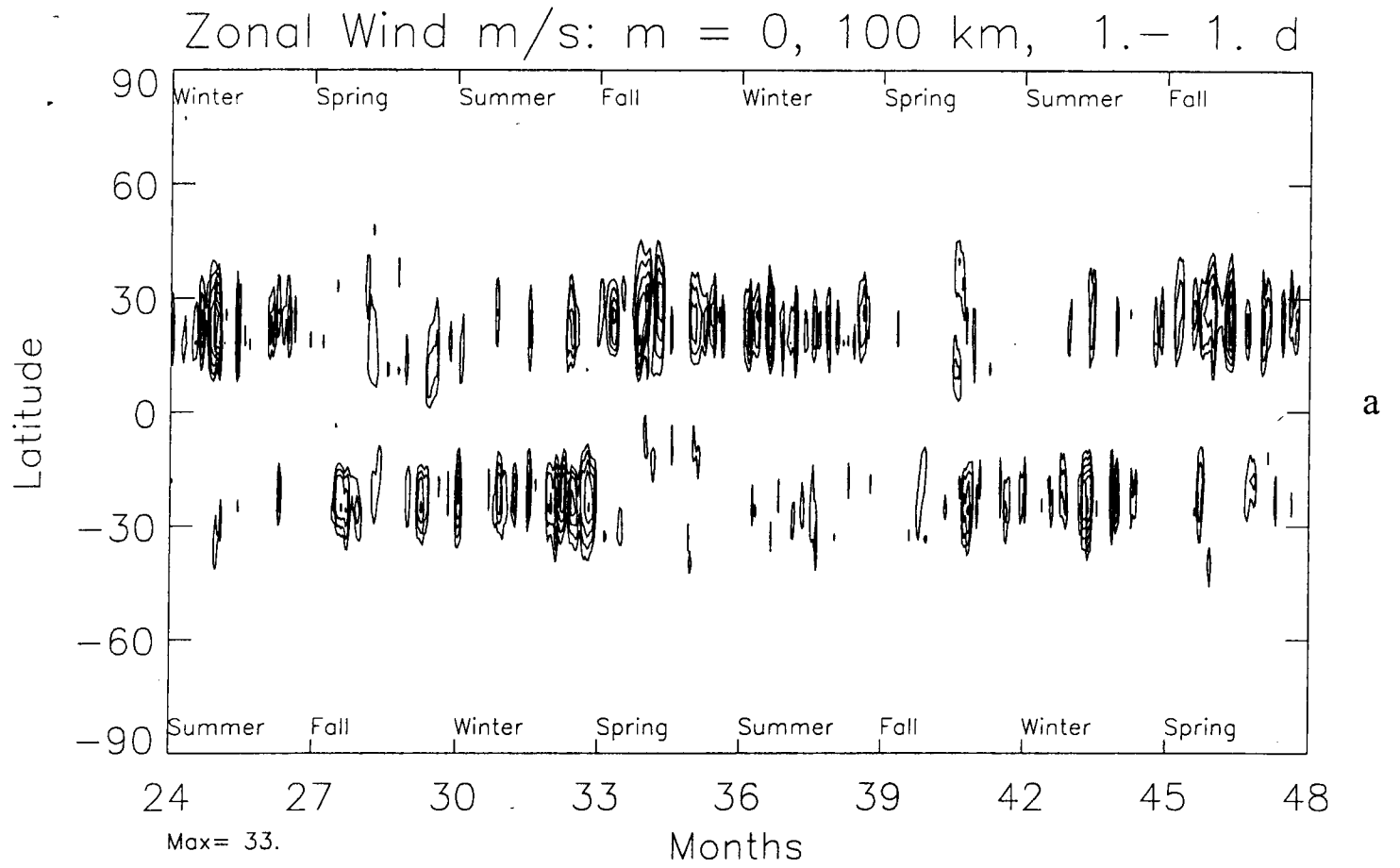
Zonal Wind m/s: m = 0, 100 km, 1.– 1. d
Winter
Spring
Summer
Fall
Winter
Spring
Summer
Fall
90
60
30
0
−30
−60
−90
Latitude
Summer
Fall
Winter
Spring
Summer
Fall
Winter
Spring
24
27
30
33
36
39
42
45
48
Max= 33.
Months

a

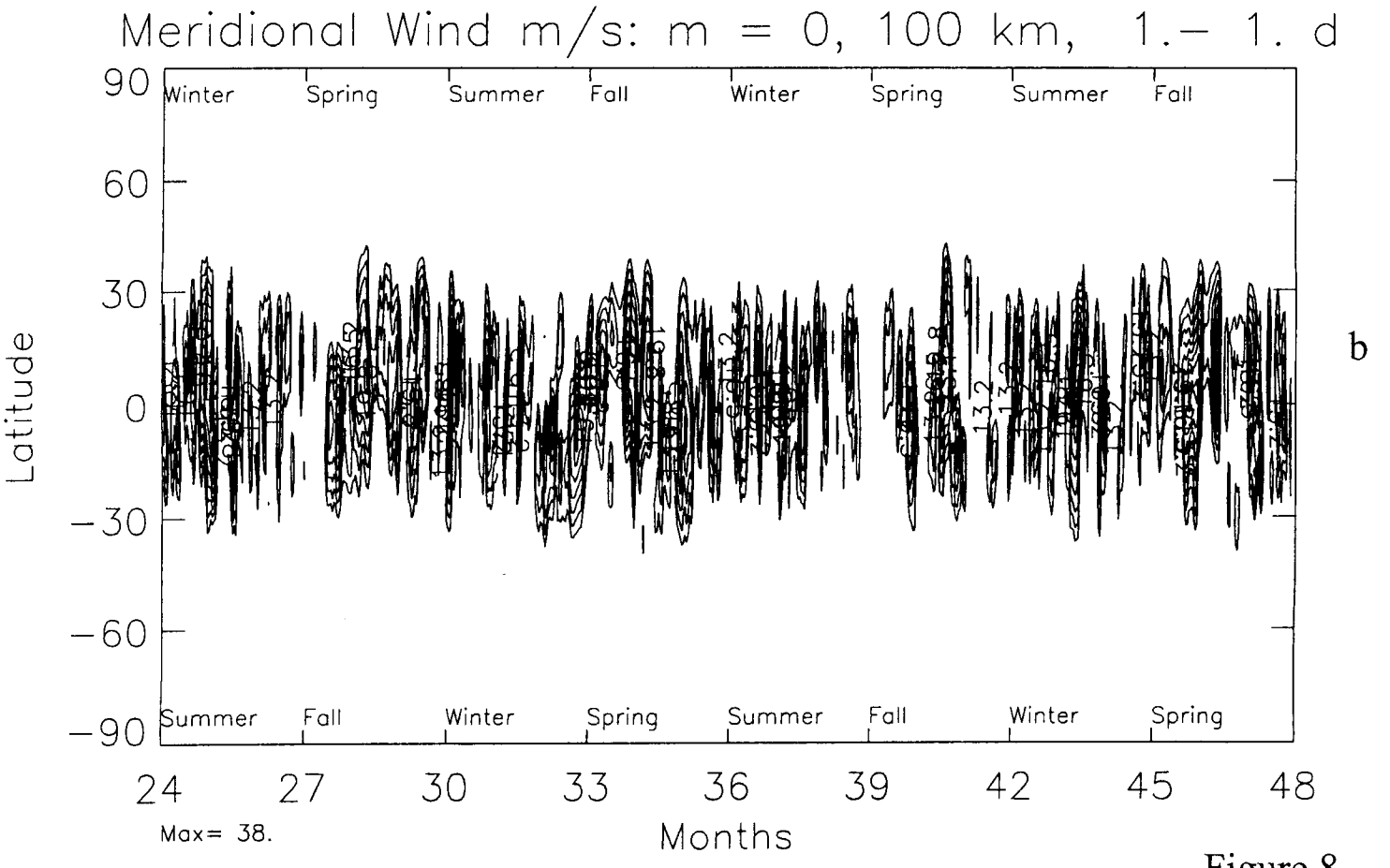
Meridional Wind m/s: m = 0, 100 km, 1.– 1. d
Winter
Spring
Summer
Fall
Winter
Spring
Summer
Fall
90
60
30
0
−30
−60
−90
Latitude
Summer
Fall
Winter
Spring
Summer
Fall
Winter
Spring
24
27
30
33
36
39
42
45
48
Max= 38.
Months
cut=4 nwd=2 C290

b

Figure 8

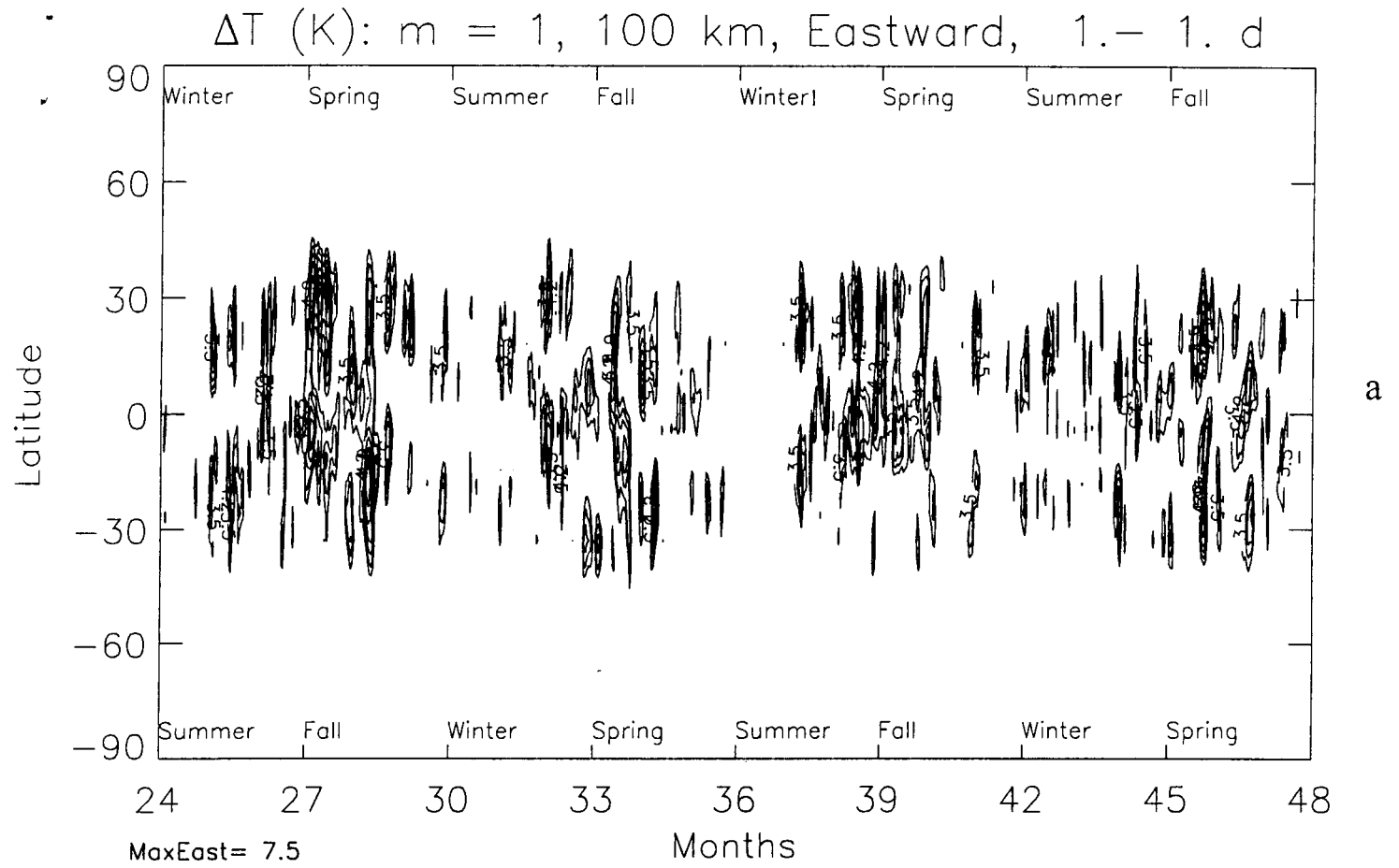
ΔT (K): m = 1, 100 km, Eastward, 1.– 1. d
Winter
Spring
Summer
Fall
Winter
Spring
Summer
Fall
Summer
Fall
Winter
Spring
Summer
Fall
Winter
Spring
90
60
30
0
−30
−60
−90
Latitude
24
27
30
33
36
39
42
45
48
Months
MaxEast= 7.5

a

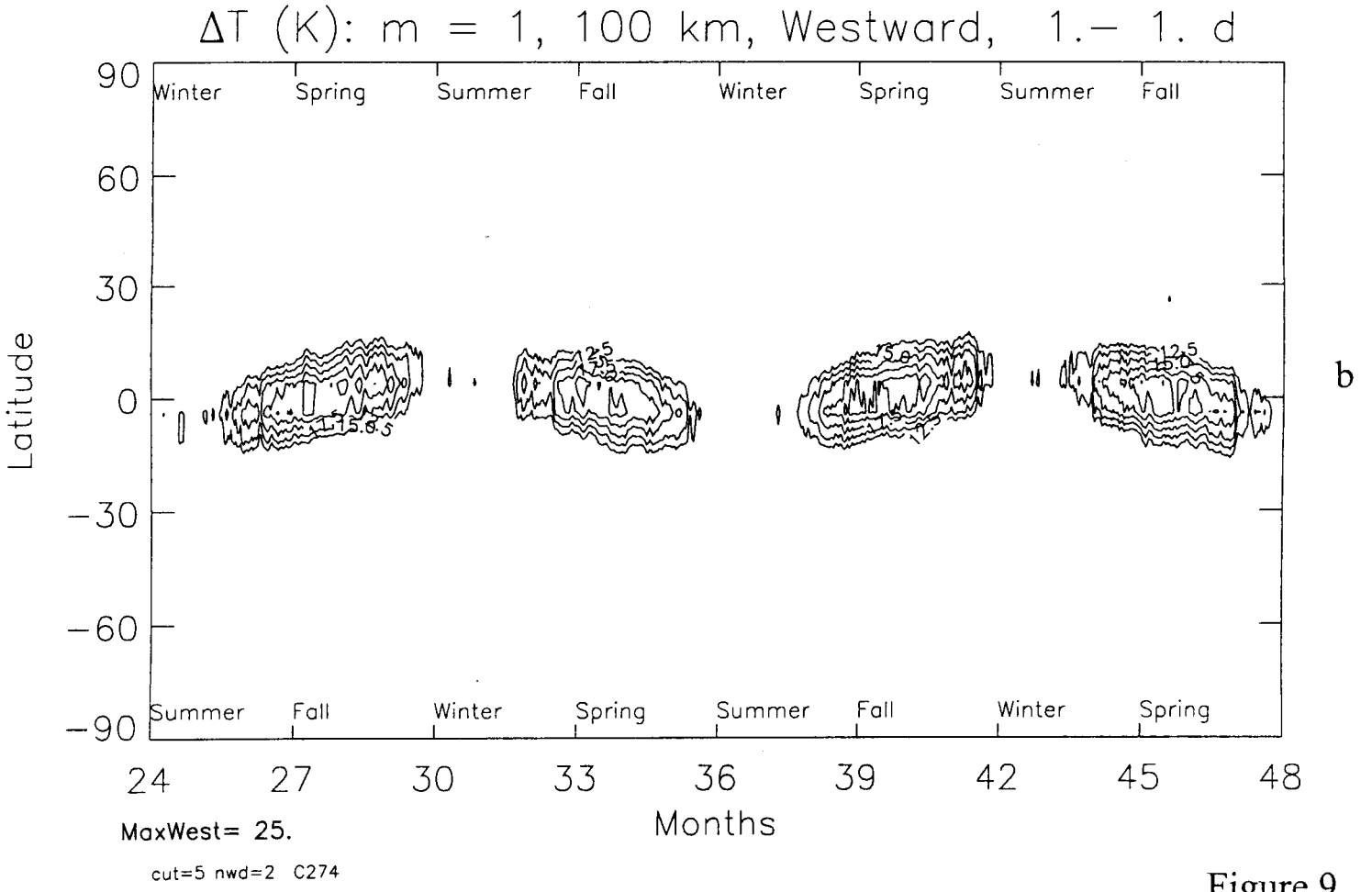
ΔT (K): m = 1, 100 km, Westward, 1.– 1. d
Winter
Spring
Summer
Fall
Winter
Spring
Summer
Fall
Summer
Fall
Winter
Spring
Summer
Fall
Winter
Spring
90
60
30
0
−30
−60
−90
Latitude
24
27
30
33
36
39
42
45
48
Months
MaxWest= 25.
cut=5 nwd=2 C274

b

Figure 9

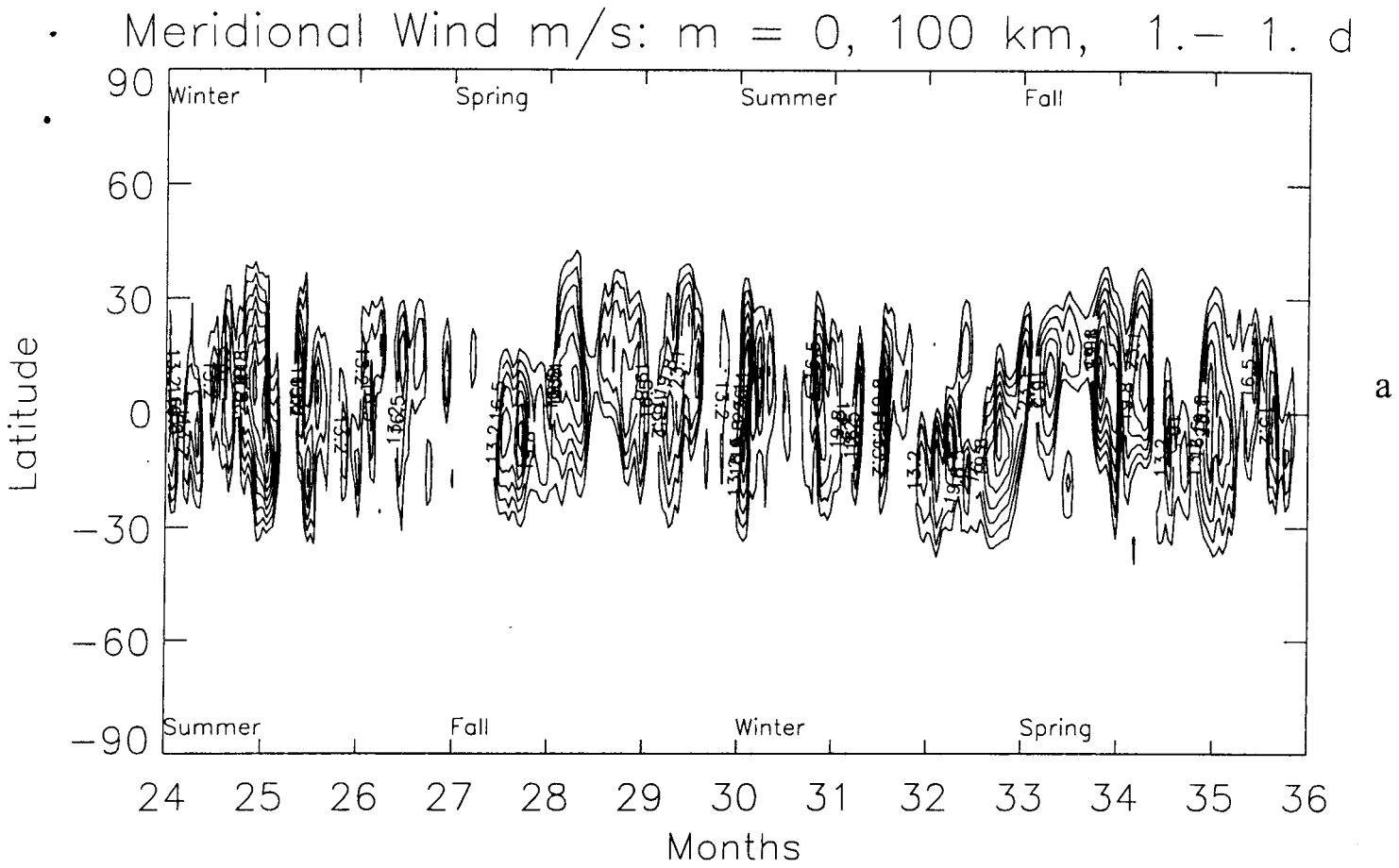
Meridional Wind m/s: m = 0, 100 km, 1.– 1. d
Winter
Spring
Summer
Fall
Summer
Fall
Winter
Spring
Latitude
90
60
30
0
−30
−60
−90
24 25 26 27 28 29 30 31 32 33 34 35 36
Months
Max= 38.

a

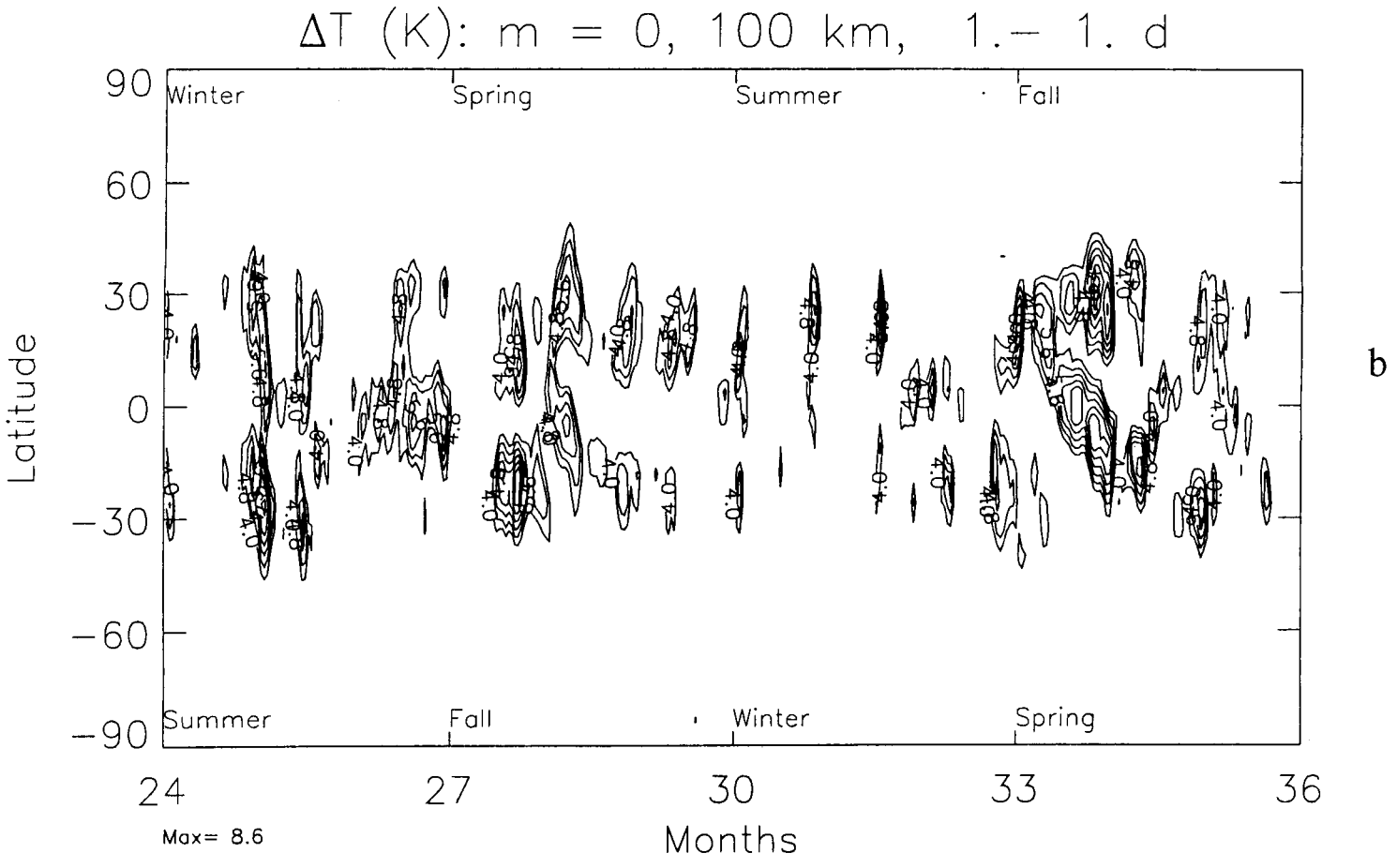
ΔT (K): m = 0, 100 km, 1.– 1. d
Winter
Spring
Summer
Fall
Summer
Fall
Winter
Spring
Latitude
90
60
30
0
−30
−60
−90
24 27 30 33 36
Months
Max= 8.6
cut=5 nwd=2 C278

b

Figure 10

Semi-diurnal Tides (12 hour)

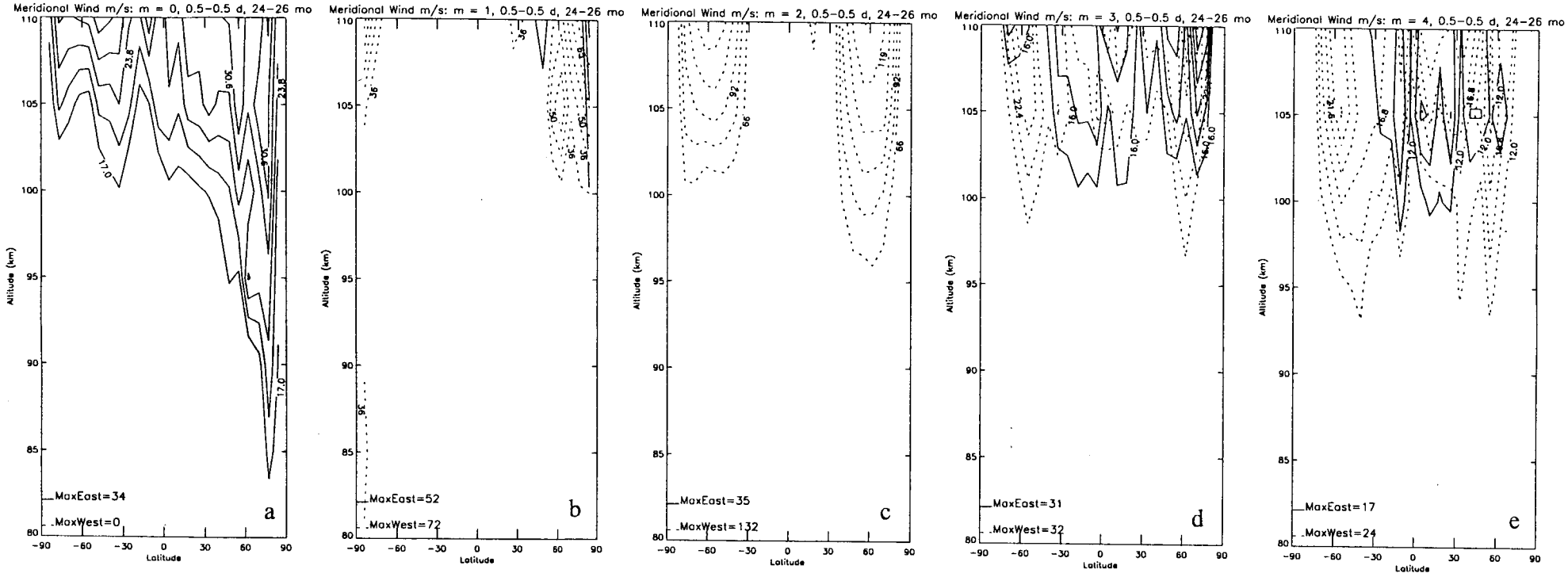

Figure 11

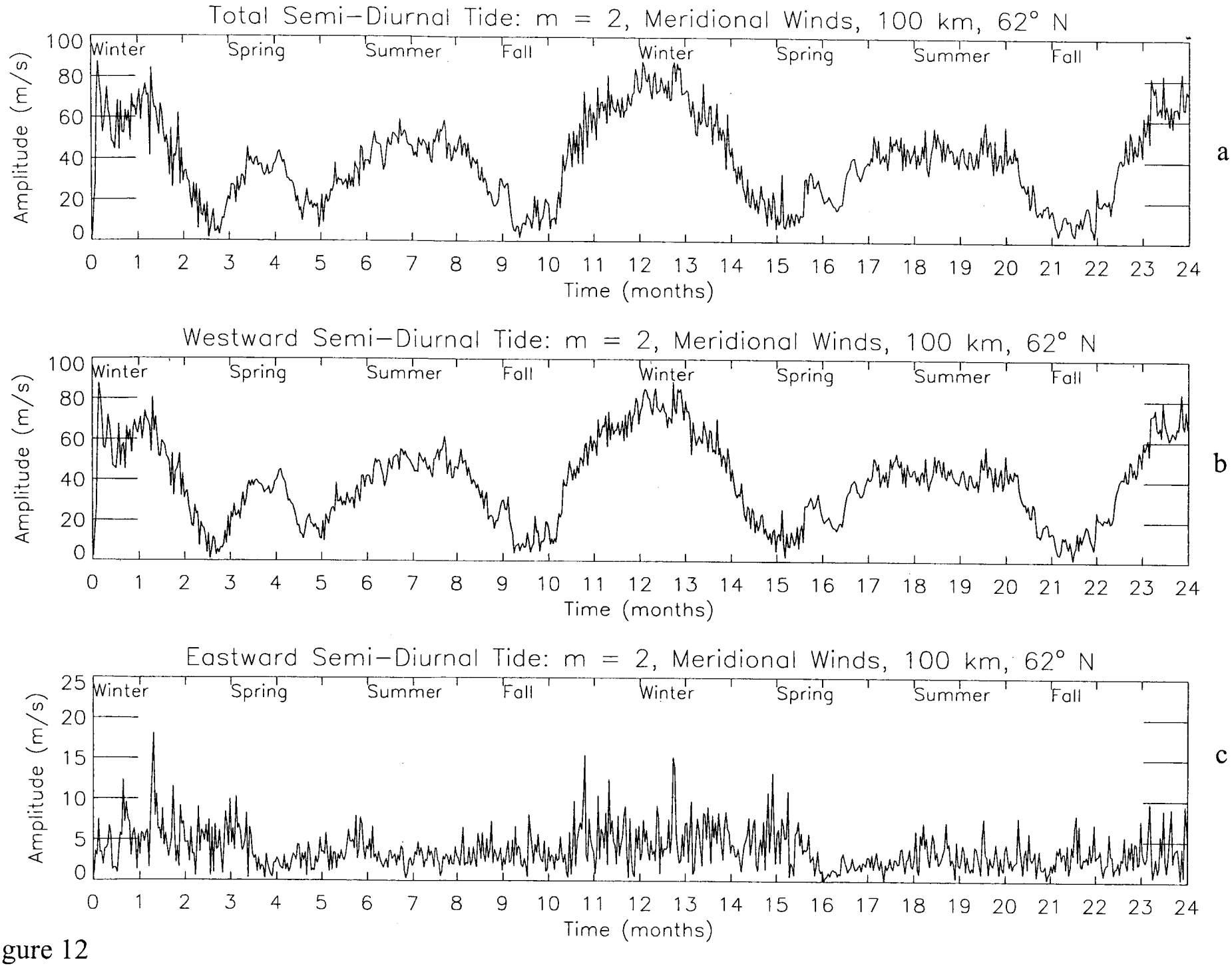
Total Semi−Diurnal Tide: m = 2, Meridional Winds, 100 km, 62° N
Westward Semi−Diurnal Tide: m = 2, Meridional Winds, 100 km, 62° N
Eastward Semi−Diurnal Tide: m = 2, Meridional Winds, 100 km, 62° N
Winter
Spring
Summer
Fall
Amplitude (m/s)
Time (months)
a
b
c

Figure 12

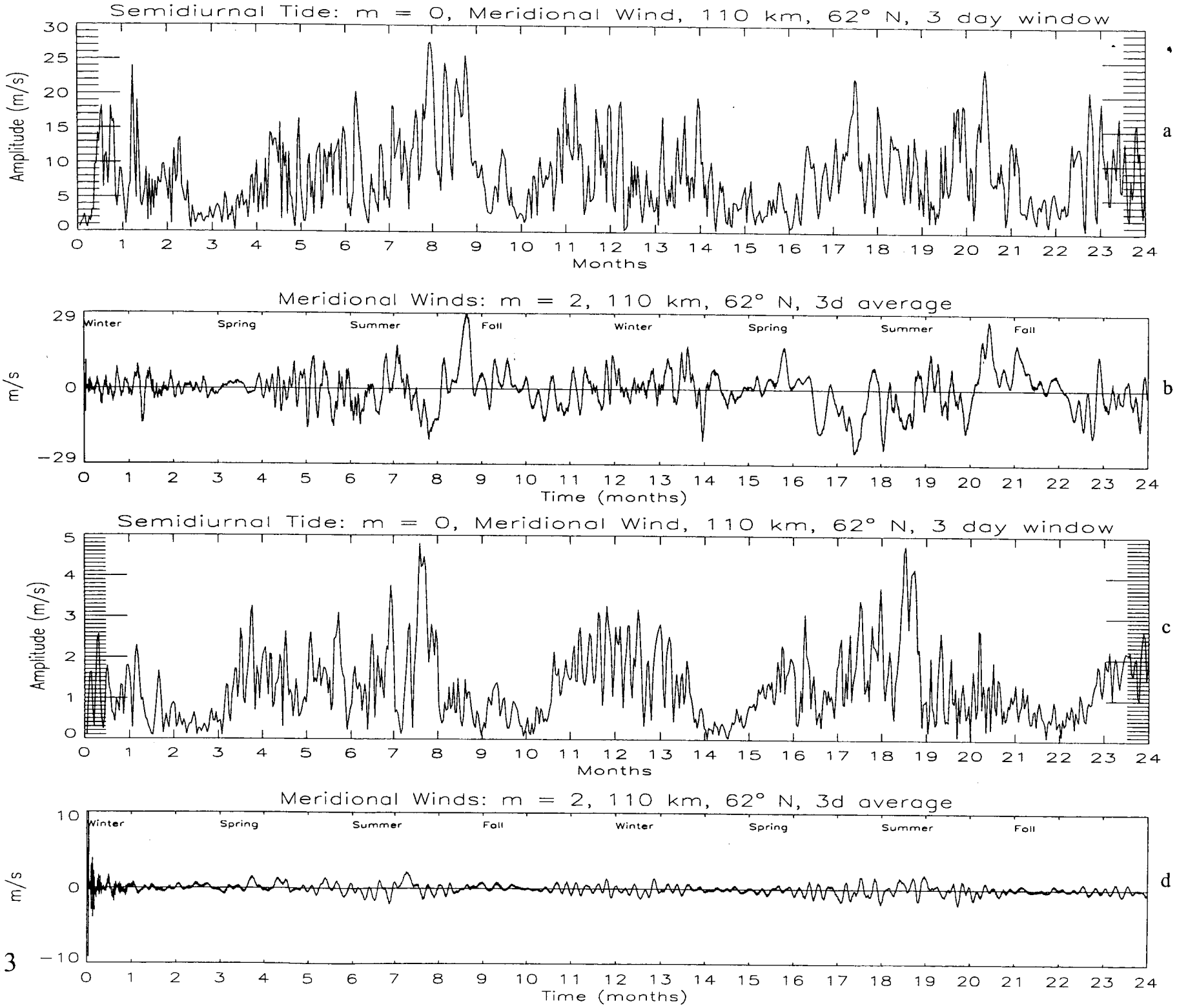
Semidiurnal Tide: m = 0, Meridional Wind, 110 km, 62° N, 3 day window
Amplitude (m/s)
Months
a
Meridional Winds: m = 2, 110 km, 62° N, 3d average
Winter
Spring
Summer
Fall
m/s
Time (months)
b
Semidiurnal Tide: m = 0, Meridional Wind, 110 km, 62° N, 3 day window
Amplitude (m/s)
Months
c
Meridional Winds: m = 2, 110 km, 62° N, 3d average
Winter
Spring
Summer
Fall
m/s
Time (months)
d

Figure 13

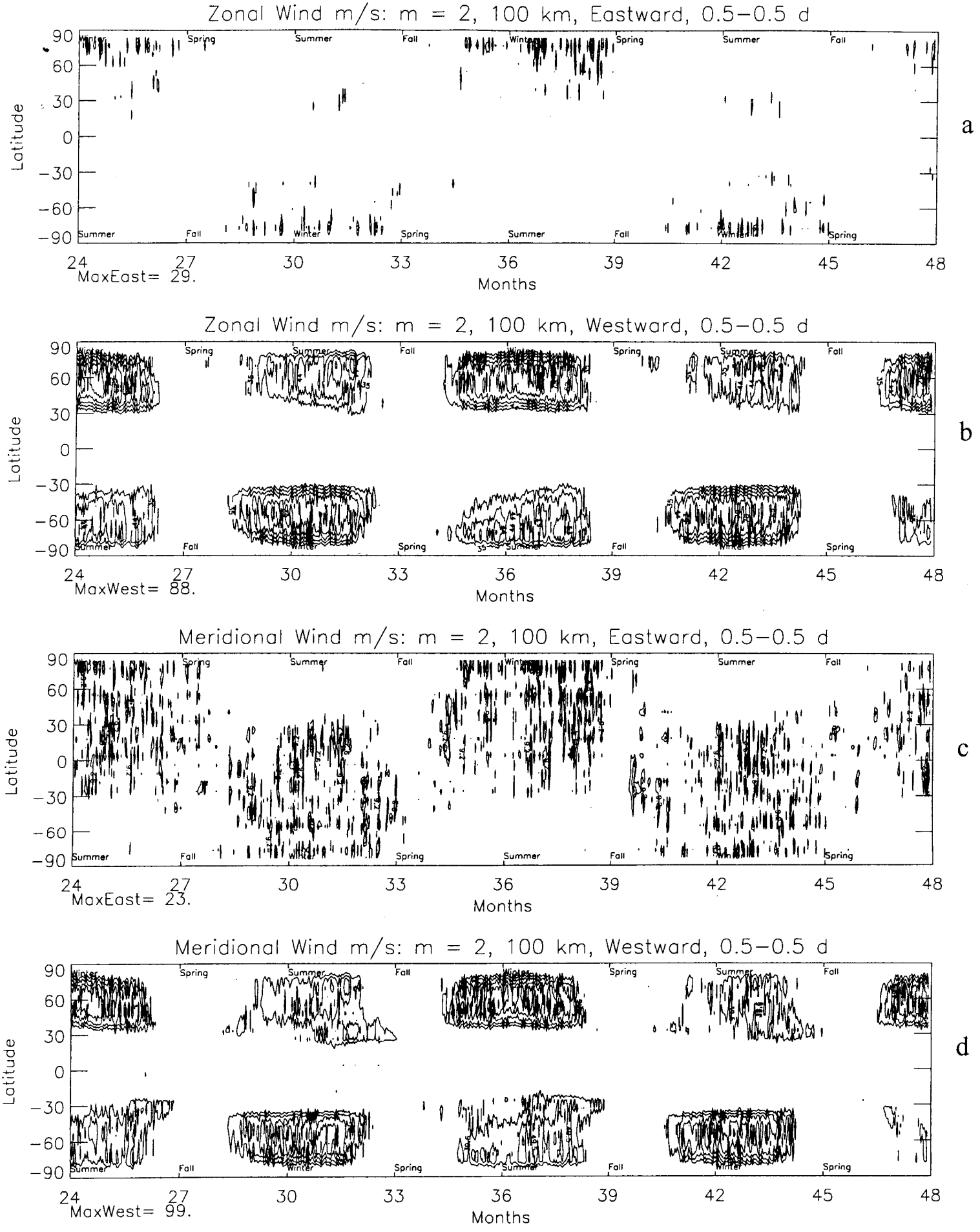
Zonal Wind m/s: m = 2, 100 km, Eastward, 0.5–0.5 d
Latitude
Months
MaxEast= 29.
a
Zonal Wind m/s: m = 2, 100 km, Westward, 0.5–0.5 d
Latitude
Months
MaxWest= 88.
b
Meridional Wind m/s: m = 2, 100 km, Eastward, 0.5–0.5 d
Latitude
Months
MaxEast= 23.
c
Meridional Wind m/s: m = 2, 100 km, Westward, 0.5–0.5 d
Latitude
Months
MaxWest= 99.
d

Figure 14

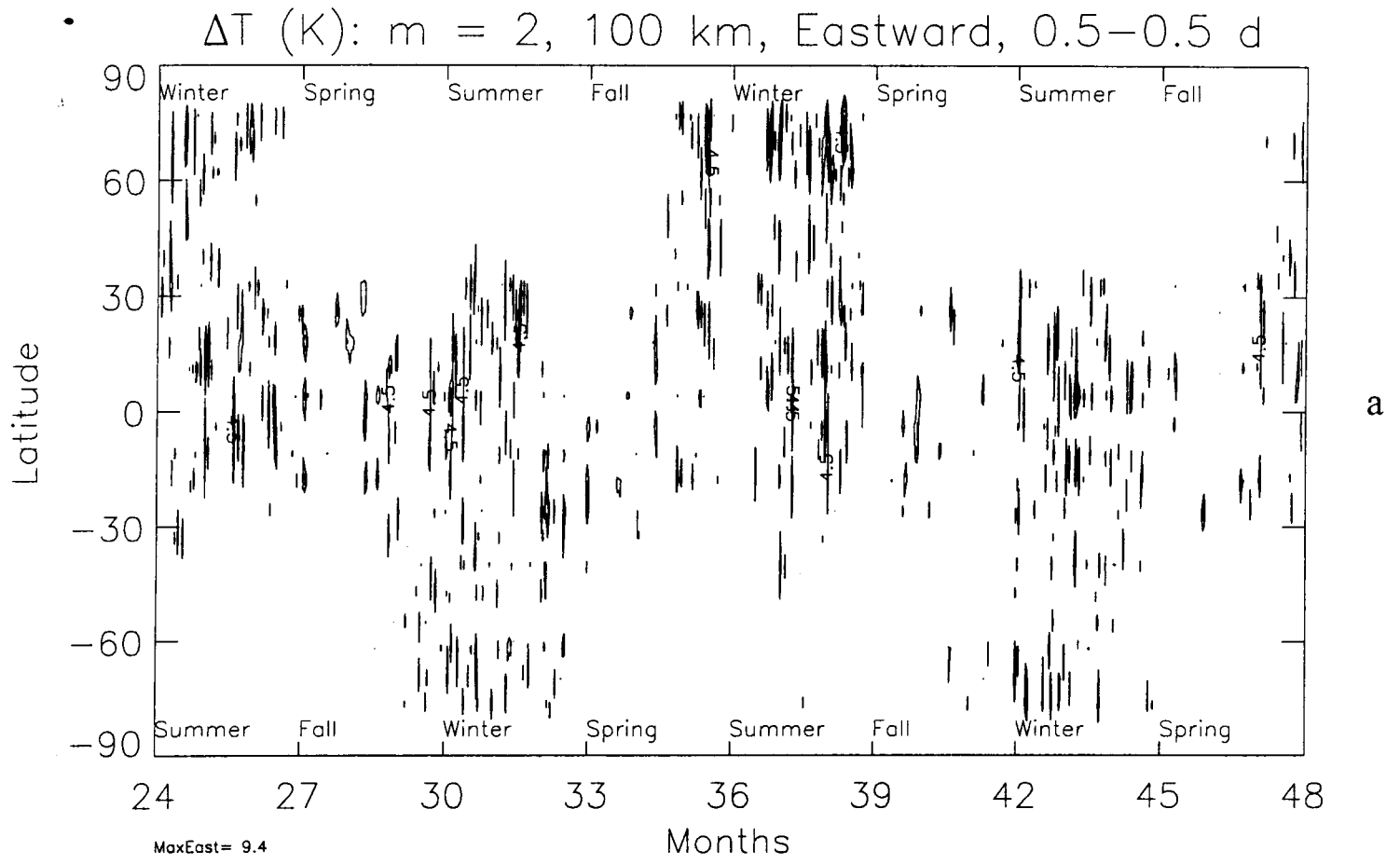
ΔT (K): m = 2, 100 km, Eastward, 0.5–0.5 d
Winter
Spring
Summer
Fall
Winter
Spring
Summer
Fall
90
60
30
0
−30
−60
−90
Latitude
Summer
Fall
Winter
Spring
Summer
Fall
Winter
Spring
24
27
30
33
36
39
42
45
48
Months
MaxEast= 9.4

a

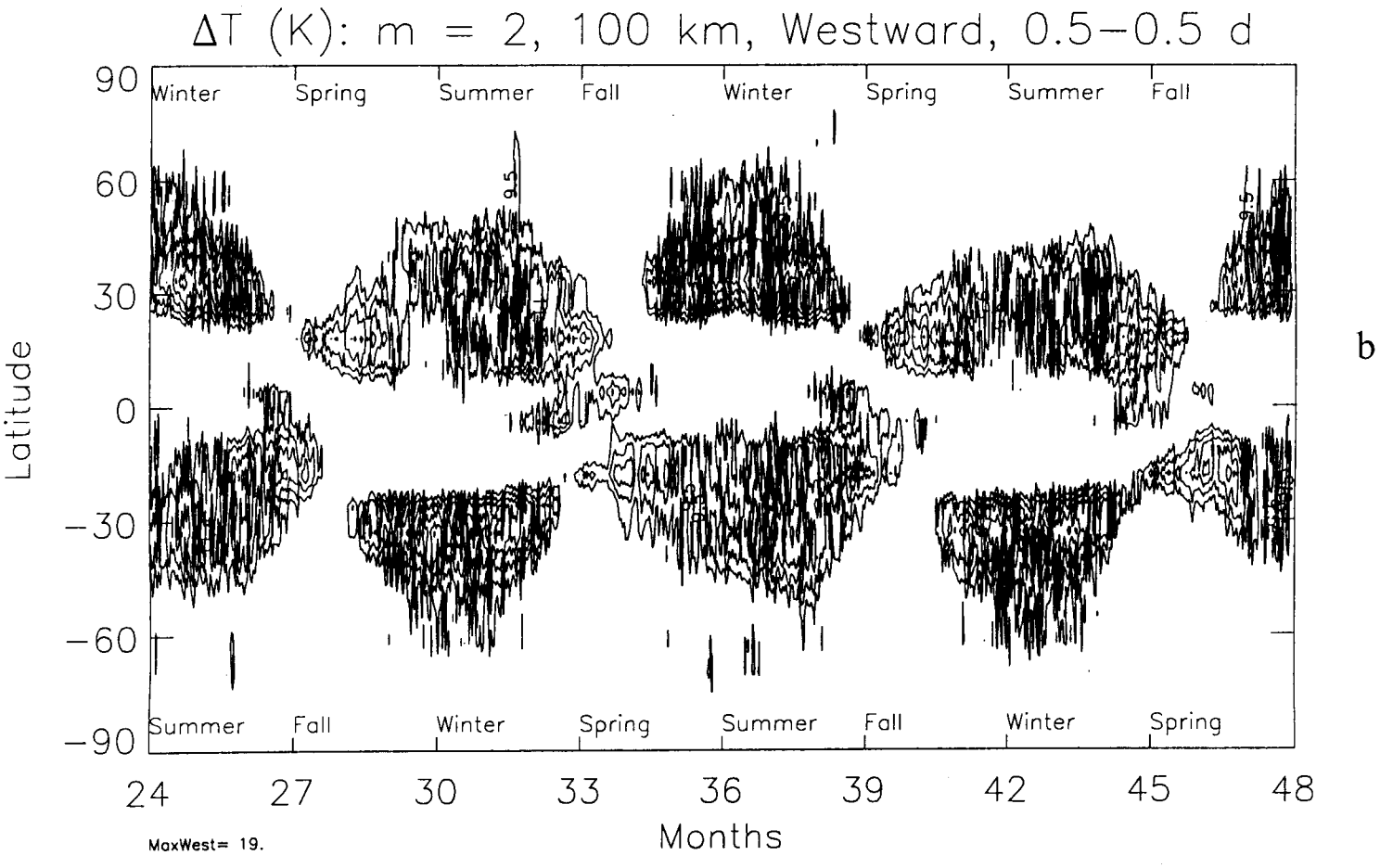
ΔT (K): m = 2, 100 km, Westward, 0.5–0.5 d
Winter
Spring
Summer
Fall
Winter
Spring
Summer
Fall
90
60
30
0
−30
−60
−90
Latitude
Summer
Fall
Winter
Spring
Summer
Fall
Winter
Spring
24
27
30
33
36
39
42
45
48
Months
MaxWest= 19.
cut=5 nwd=2 C283

b

Figure 15

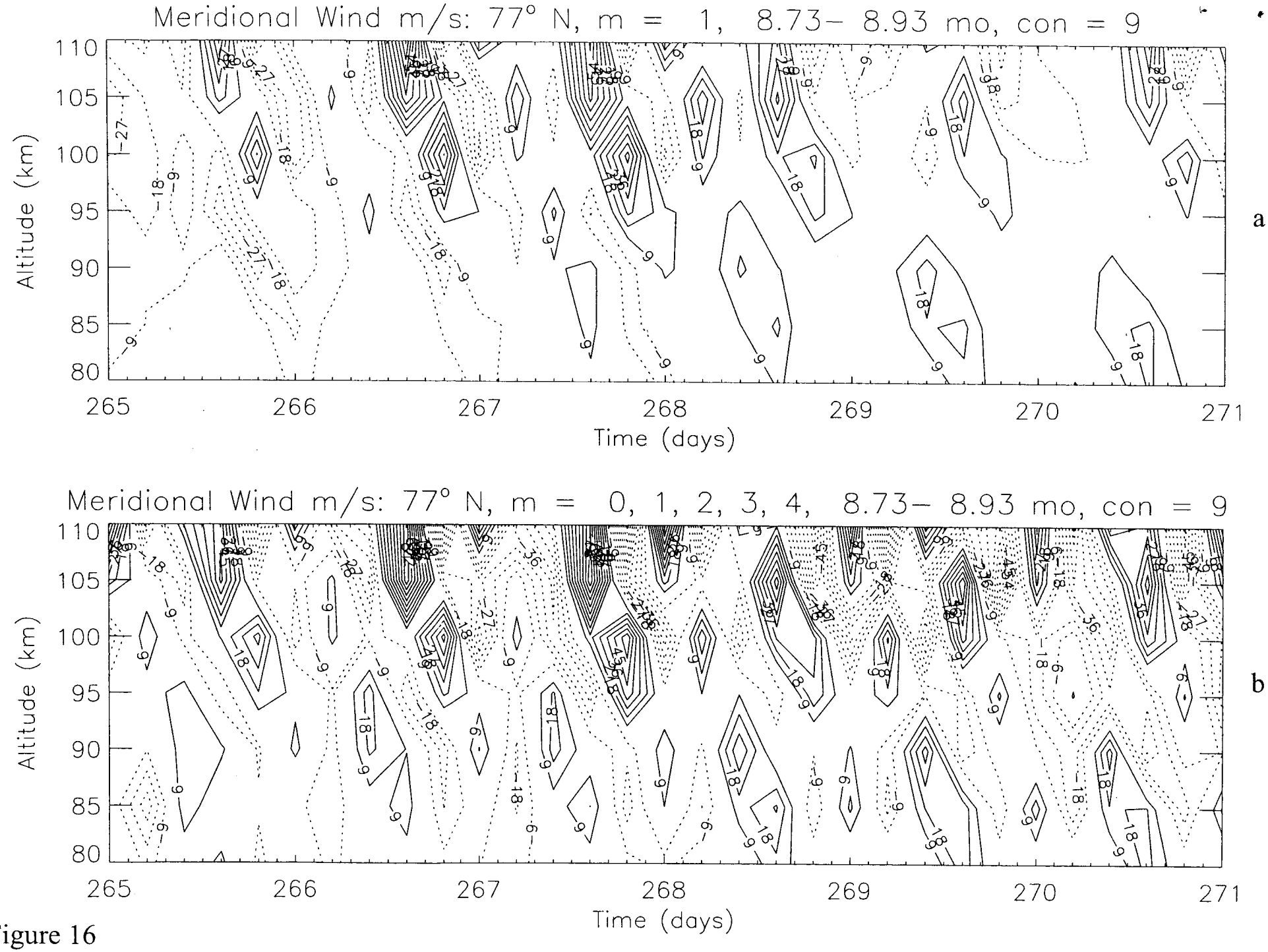
Meridional Wind m/s: 77° N, m = 1, 8.73– 8.93 mo, con = 9
Altitude (km)
110
105
100
95
90
85
80
265
266
267
268
269
270
271
Time (days)
a
Meridional Wind m/s: 77° N, m = 0, 1, 2, 3, 4, 8.73– 8.93 mo, con = 9
Altitude (km)
Time (days)
b

Figure 16

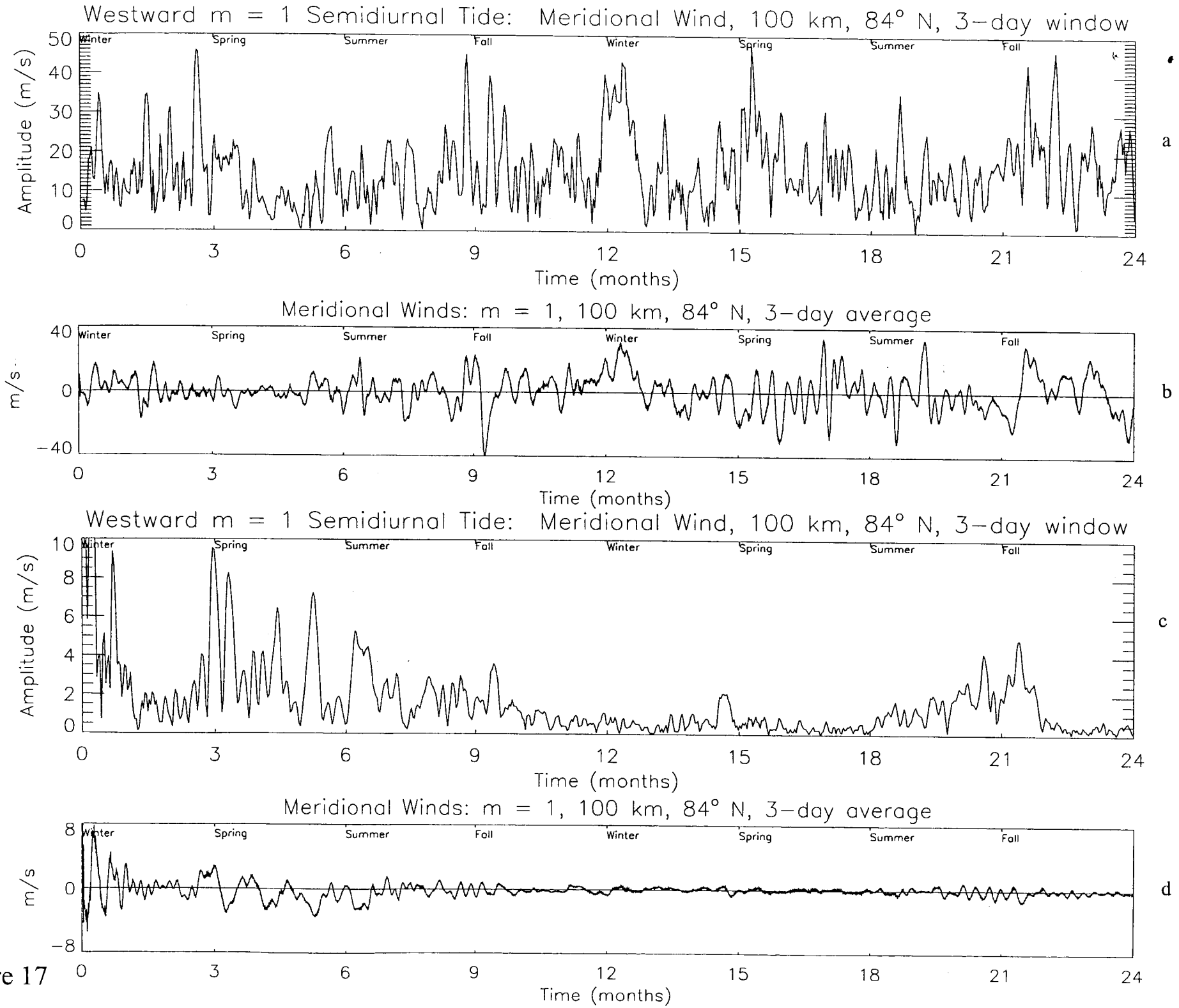
Westward m = 1 Semidiurnal Tide: Meridional Wind, 100 km, 84° N, 3-day window
Amplitude (m/s)
Winter
Spring
Summer
Fall
Time (months)
a
Meridional Winds: m = 1, 100 km, 84° N, 3-day average
m/s
b
Westward m = 1 Semidiurnal Tide: Meridional Wind, 100 km, 84° N, 3-day window
c
Meridional Winds: m = 1, 100 km, 84° N, 3-day average
d

Figure 17

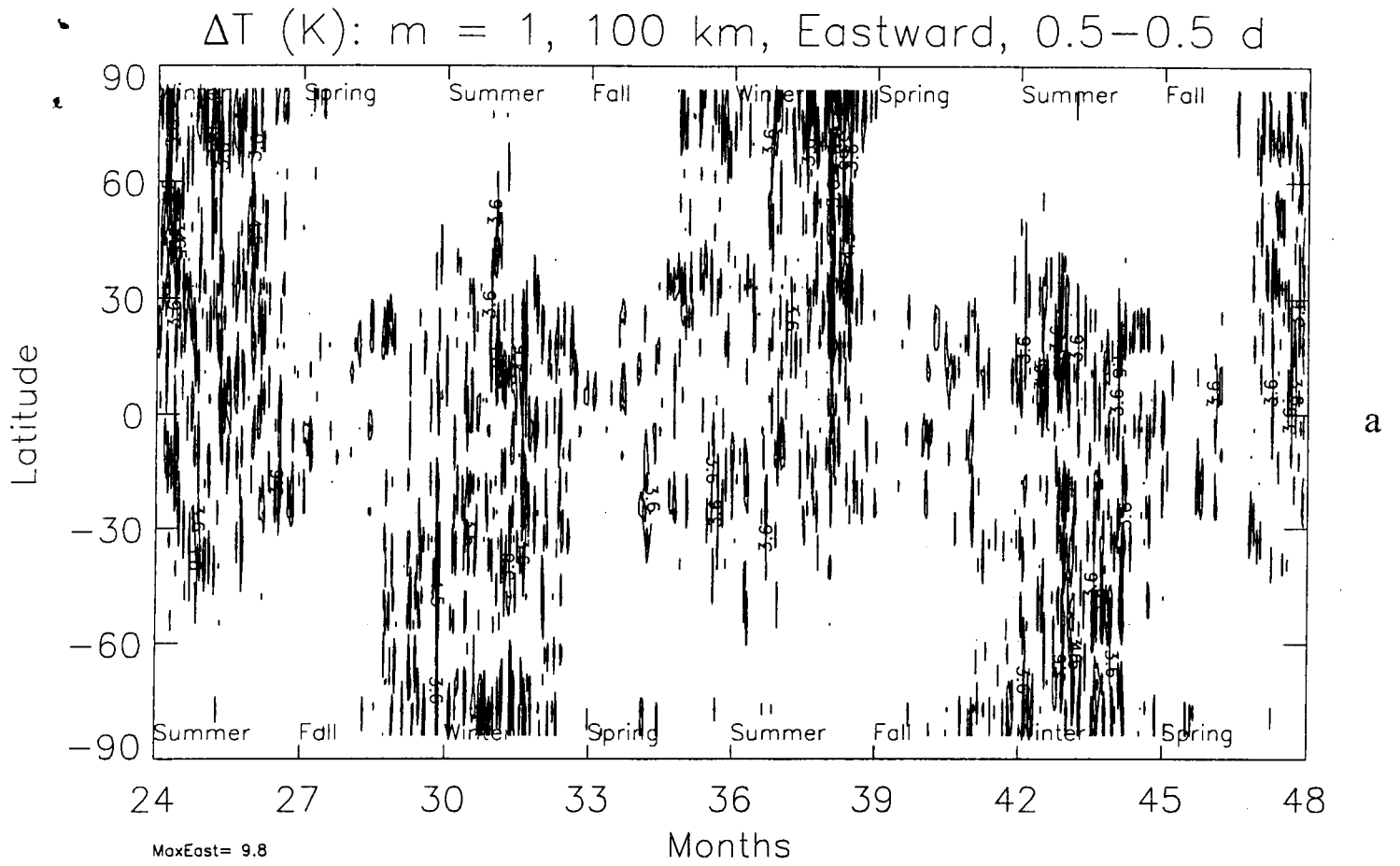
ΔT (K): m = 1, 100 km, Eastward, 0.5–0.5 d
Winter
Spring
Summer
Fall
Winter
Spring
Summer
Fall
Summer
Fall
Winter
Spring
Summer
Fall
Winter
Spring
90
60
30
0
−30
−60
−90
Latitude
24
27
30
33
36
39
42
45
48
Months
MaxEast= 9.8

a

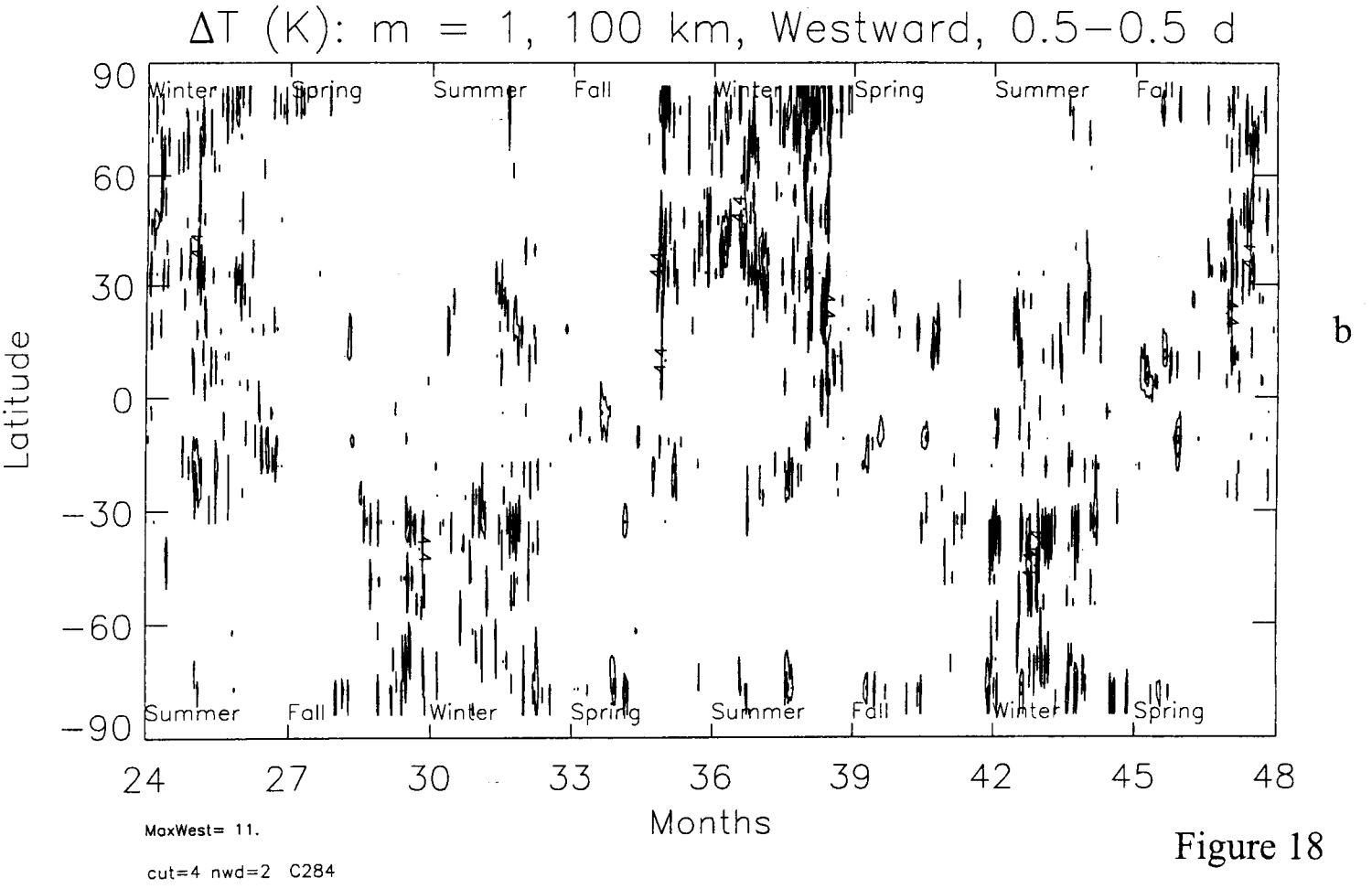
ΔT (K): m = 1, 100 km, Westward, 0.5–0.5 d
Winter
Spring
Summer
Fall
Winter
Spring
Summer
Fall
Summer
Fall
Winter
Spring
Summer
Fall
Winter
Spring
90
60
30
0
−30
−60
−90
Latitude
24
27
30
33
36
39
42
45
48
Months
MaxWest= 11.
cut=4 nwd=2 C284

b

Figure 18

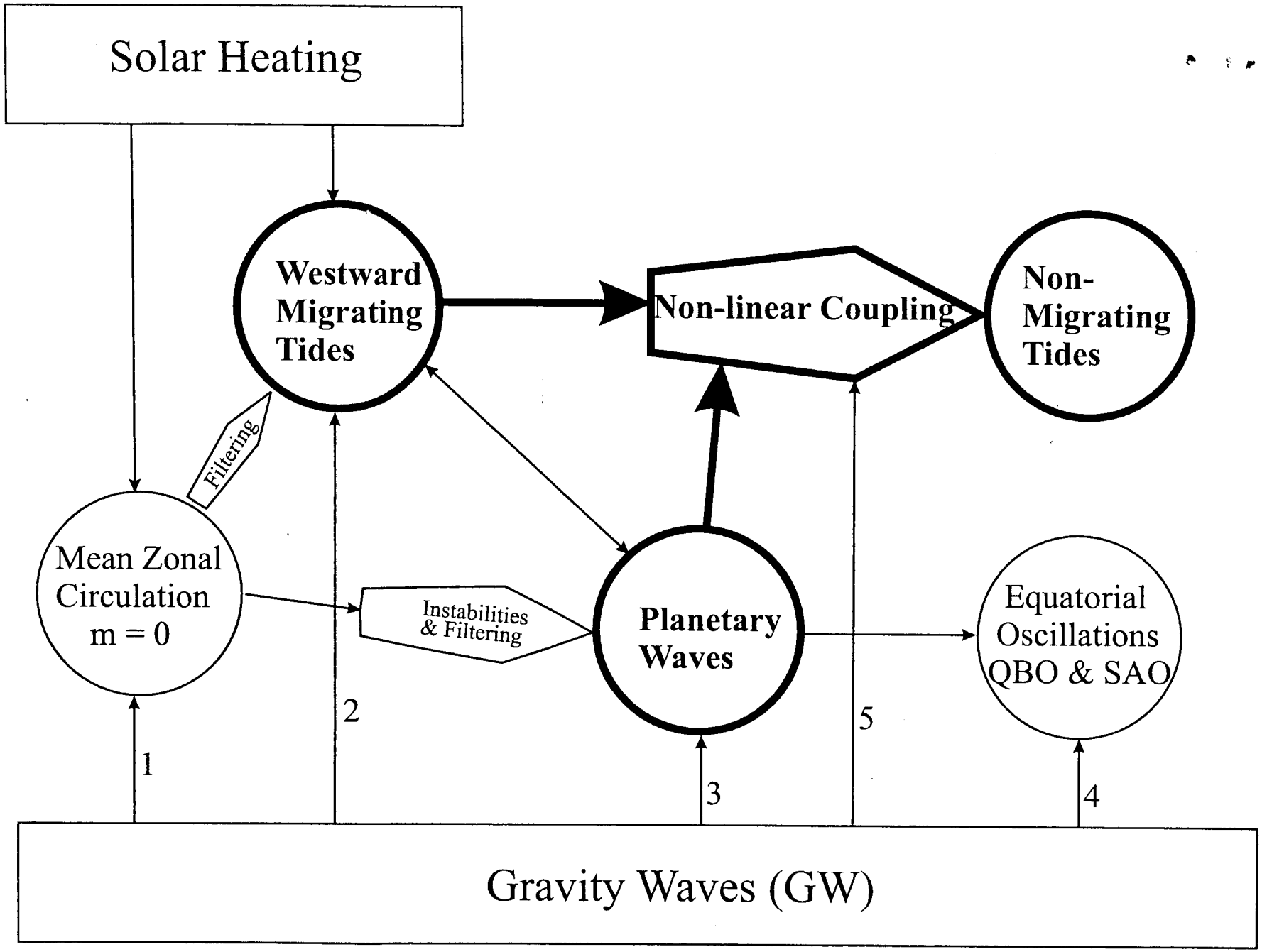

(1) GW interaction produces temperature and wind reversals that lead to instabilities
(2) GW interaction amplifies tides
(3) GW interaction amplifies planetary waves
(4) GW source of QBO and SAO
(5) GW filtering contributes to non-linear coupling

Figure 19